Diagrammatic approach to meson-meson scattering in the nonrelativistic quark potential model

T. Barnes

Physics Division and Center for Computationally Intensive Physics, Oak Ridge National Laboratory,
Oak Ridge, Tennessee 37831-6373
and Department of Physics, University of Tennessee, Knoxville, Tennessee 37996-1200

E. S. Swanson

Center for Theoretical Physics, Massachusetts Institute of Technology, Cambridge, Massachusetts 02139
(Received 5 December 1991)

In this paper we use Born-order quark-exchange diagrams in a nonrelativistic potential model to describe low-energy scattering of $q\bar{q}$ mesons. A formalism for evaluating quark Born diagrams is developed, and as a first application we consider meson-meson scattering in channels in which $q\bar{q}$ annihilation is thought to be unimportant. In particular our results are relevant to $I = 2$ $\pi\pi$ and $I = 1$ KK elastic scattering. Simple rules for the Born diagrams are given, which allow the evaluation of scattering amplitudes in terms of external meson wave functions by inspection. These techniques are applied to systems having identical quarks, and $\pi^+\pi^+$, K^+K^+, and $\rho^+\rho^+$ elastic scattering phase shifts, cross sections, and equivalent potentials are derived as examples. The S-wave $I = 2$ $\pi\pi$ phase shift for a Gaussian $q\bar{q}$ wave function with conventional quark model parameters α_s, m_q, and $\beta_{\rm SHO}$ is found to be in good agreement with experiment and with Weinberg's PCAC (partial conservation of axial-vector current) result. At higher energies the predicted differential cross sections have the characteristic diffractive features of an exponential t peak at small angles and vacuum quantum number exchange. The phase of the predicted amplitude however differs from the experimental diffractive amplitude, so these quark Born diagrams cannot be directly identified with the "Pomeron" of diffractive scattering phenomenology.

PACS number(s): 13.75.Lb, 12.40.Qq

I. INTRODUCTION

Even a cursory investigation reveals that hadron scattering at low energies is a very complicated process. Experimental studies have shown that important contributions can arise from s-channel resonance production, t-channel resonance exchange, and nonresonant scattering. Theoretical attempts to describe experimental results for hadron scattering have used a wide variety of methods, ranging from the application of general principles such as analyticity and dispersion relations to detailed dynamical models involving meson exchange, quark and gluon exchange, and most recently lattice gauge theory. Indeed, the literature on hadron scattering is so extensive that we must restrict our introduction to a brief discussion of research which appears most closely related to the perturbative techniques we have developed.

One reason for the difficulty of describing hadron scattering is the strength of the strong interaction at low energies, which as a meson-baryon effective interaction appears to be nonperturbatively large. Perhaps the most familiar example of such large couplings is the pion-nucleon effective coupling constant, which was estimated to be ≈ 15 in pion-exchange models of the nuclear interaction [1] in the 1950s. Although this leads one to doubt the validity of perturbative calculations involving effective hadron fields, soft-pion amplitudes including the S-wave $\pi\pi$ scattering lengths have been successfully described us-

ing PCAC (partial conservation of axial-vector current) [2]. In part because of the strength of the strong interaction, analytic continuation approaches are at present the most accurate techniques available for relating meson-meson scattering amplitudes; in particular, the recent work of Au, Morgan, and Pennington [3] has been very successful in relating various reactions involving $\pi\pi$ systems. Unfortunately, this approach does not provide a detailed dynamical model of the mechanism underlying hadron scattering.

As there is clear evidence for one-pion exchange in the t distributions of many strong processes, meson-exchange models of strong forces have been developed for several systems, the most familiar being the nucleon-nucleon system [4]. These models have attributed the strong repulsive core of the nucleon-nucleon interaction to exchange of vector mesons such as the $\omega(783)$. This now appears incorrect; a G-parity transformation applied to vector exchange predicts an attractive core for the nucleon-antinucleon interaction and corresponding deeply bound states [5], and such states have not been seen experimentally at $p\bar{p}$ facilities such as the CERN Low Energy Antiproton Ring (LEAR). A plausible explanation for the failure of these predictions is that vector-meson exchange is actually unimportant, since the corresponding forces would have a range of only 0.2 fm, much smaller than the 2-fm separation required for two distinct nucleons [6]. Meson-exchange models presumably

are parametrizations of other mechanisms, which should be more evident at the quark and gluon level.

Although the development of the quark model and QCD made hadron scattering a more well defined problem, the difficulty of calculating scattering amplitudes of multiquark systems has delayed progress in the description of low-energy hadron scattering in terms of fundamental QCD constituents. The technique most often used is the resonating group method, and more recently there have been several variational studies; both methods require considerable theoretical effort when applied to hadron scattering problems. Because of its fundamental importance to nuclear physics, the two-nucleon system has been the subject of many investigations using six-quark wave functions; the extensive literature on this subject has recently been reviewed by Shimizu [7]. Calculations published by Liberman [8] in 1977 (using the nonrelativistic quark potential model) and DeTar [9] (using the bag model) in 1978 found the dominant short-distance repulsive core from the interaction of quark wave functions without requiring vector-meson exchange. More recent work by Maltman and Isgur [10] in the nonrelativistic quark potential model further concluded that the intermediate-range attraction could be explained as a spatial distortion of the three-quark clusters rather than as an effect of pion exchange. Liberman, Shimizu, Maltman, and Isgur all conclude that the dominant repulsive core is due to the color-magnetic (spin-spin) component of one-gluon exchange, which is then followed by quark exchange to restore color-singlet states. In this paper we shall assume that the same mechanism dominates nonresonant meson-meson scattering, and find that it gives a good description of $I = 2$ $\pi\pi$ scattering.

Meson-meson scattering has received rather less attention than the nucleon-nucleon interaction, presumably because the scattering amplitudes are less well established experimentally, and in many channels are complicated by resonance production. In early work on meson-meson scattering Jaffe and Low [11] introduced a "P-matrix" formalism for calculating hadron scattering amplitudes using bag-model wave functions; this formalism was applied to experimental meson-meson phase shifts to infer the location of P-matrix poles. A direct calculation of meson-meson scattering amplitudes from bag-model wave functions using the P-matrix formalism however has not been published. In the high-energy regime, meson-meson scattering in perturbative QCD has been studied by Brodsky, Lepage, and collaborators [12] using a light-cone formalism. The "constituent interchange model" they employ assumes that high energy scattering is dominated by quark-exchange diagrams. Meson-meson scattering at low energies using a nonrelativistic quark model description has been studied by Weinstein and Isgur [13, 14]. They used a variational approach to optimize a $q^2\bar{q}^2$ wave function in a Coulomb-plus-linear potential with a hyperfine term, and projected the $q^2\bar{q}^2$ state onto free $q\bar{q}$ wave functions to estimate a relative two-meson wave function; this gives an equivalent meson-meson potential. These potentials apparently have an underestimated range, so Weinstein and Isgur adjust their overall ranges and normalizations. This

ad hoc two-parameter scaling leads to scattering amplitudes which are in good agreement with experimental meson-meson phase shifts and inelasticities in the exotic channels of the pseudoscalar-pseudoscalar sector. (These channels are presumably free of complications due to *s*-channel resonances.) To date results have been published only for the S-wave pseudoscalar-pseudoscalar sector with u, d, and s quarks and antiquarks. Although this variational approach gives a reasonable description of meson-meson scattering amplitudes, it requires considerable effort in the variational calculation of the multiquark ground state. As a variational method, its applications are limited to the lowest-lying meson-meson states in each sector of Hilbert space. One may also object to the rather arbitrary projection of this four-quark wave function onto two free mesons to obtain an approximate two-meson wave function, and to the scaling of the meson-meson potentials. Although this scaling is necessary to obtain agreement with experiment, it nonetheless represents a reinterpretation of results which, as derived, are in disagreement with experiment.

In this paper we also discuss meson-meson scattering in the context of the nonrelativistic quark potential model. In particular, we investigate the attractive possibility that results similar to the scaled variational potentials of Weinstein and Isgur can be obtained from Born-order quark scattering diagrams. There is much circumstantial evidence that high-order diagrams are relatively unimportant in hadron spectroscopy and in low-energy scattering and decays (excluding $u\bar{u} \leftrightarrow d\bar{d}$ mixing). In spectroscopy, if higher-order diagrams were important one would expect resonances to be complicated mixtures in flavor space. Such higher-order flavor mixing is known to be relatively unimportant in experimentally well-established hadrons, with the exception of the pseudoscalar states $\eta(549)$ and $\eta'(957)$. The complete mixing of u and d quark states to produce isospin eigenstates is in contrast evidence that the effects of higher-order $u\bar{u} \leftrightarrow d\bar{d}$ mixing diagrams are large relative to the *u-d* quark mass difference.

Motivated by this evidence for low-order QCD dominance and by the conclusions of studies of the nucleon-nucleon interaction, we calculate meson-meson scattering amplitudes given the simplest perturbative process: A single interaction through one-gluon exchange or the confining potential is followed by rearrangement into color-singlet final states. This is essentially the "constituent interchange" mechanism [12] augmented by one-gluon exchange. Although this is a simple mechanism, the presence of four interacting fermions with spin, flavor, and color degrees of freedom, four asymptotic meson wave functions and a crossing relation between the initial and final bases makes this a rather intricate scattering problem. We attempt to simplify the calculations by developing a diagrammatic representation, which should be useful in future applications to other processes. We do not consider production of *s*-channel resonances or *t*-channel meson exchange, or any other processes which involve $q\bar{q}$ pair creation or annihilation; these effects are beyond the scope of the present work and will be considered in future studies. Although such annihilation effects presumably

are important in kinematical regimes which allow resonance production, one can study nonannihilation hadron scattering in isolation by specializing to channels such as $I = 2$ $\pi\pi$ and $\rho\rho$ and $I = 1$ $K\bar{K}$, for which $q\bar{q}$ pair annihilation and light s-channel resonances are not expected to be important. We shall see that, at least in the $I = 2$ $\pi\pi$ channel for which accurate experimental phase shifts exist, the quark Born diagrams give an accurate description of the dominant S-wave scattering amplitude. We also show how these quark and gluon matrix elements can be related to meson-meson potentials near threshold. Our determination of nuclear forces from quark line diagrams is very similar in concept to the previous work of Gardner and Moniz [15]. A study of the phase shifts produced by our $\pi\pi$ and $K\bar{K}$ potentials suggests that the Weinstein-Isgur "rescaling" is a compensation for relativistic effects in the scattering amplitude which are lost in the extraction of potentials near threshold. We find that a large rescaling is required only in the highly relativistic $\pi\pi$ system. At higher energies we find similarities between our predicted differential cross sections and experimental diffractive scattering [16], although the phases of our predicted Born amplitude and the experimental high-energy diffractive amplitude are not in agreement [17].

We anticipate that our techniques may also prove useful in identifying channels in which final-state interactions are especially large and lead to important effects, such as the formation of "molecule" resonances of hadron pairs. Such bound states of the $K\bar{K}$ system have been discussed at length by Weinstein and Isgur [13,14]; more recently there have been suggestions that vector-meson pairs may also form deuteronlike bound states as a result of these quark-exchange potentials [18] or pion exchange [19].

The remainder of this paper is organized as follows. In Section II we describe the nonrelativistic quark potential model we use for these calculations and the $q\bar{q}$ momentum-space wave functions which are our asymptotic states. We also discuss the "post-prior" ambiguity in the definition of H_I, and derive general results for scattering amplitudes, equivalent potentials, and cross sections in terms of the matrix elements of H_I between two-meson scattering states. Section III applies this formalism to the meson-meson scattering problem. This process involves four independent H_I matrix elements, and we give a simple diagrammatic representation for each. "Capture" and "transfer" processes each account for two diagrams. These diagrams can be written as the product of flavor, color, spin, and space factors, and we illustrate the evaluation of each factor by considering a specific diagram in detail, following which we quote the full meson-meson scattering amplitude. These amplitudes are evaluated explicitly using Gaussian external wave functions. In Section IV we apply these results to $I = 2$ $\pi\pi$ and $I = 1$ $K\bar{K}$ elastic scattering; the Gaussian wave functions lead to closed-form results for differential and total cross sections and phase shifts. In the $\pi\pi$ case we compare our results to the experimental S-wave phase shift, and find good agreement over the full range of energies for which accurate data exists. We also give predictions for $I = 1$ $K\bar{K}$ elastic scattering and discuss the $I = 2$

$\rho\rho$ case. Our differential cross sections at high energies show a diffractive peak at small t, which is due to the "transfer" quark diagrams. We then give our conclusions and acknowledgments. Following this we present details of our calculations in five appendices. These appendices discuss (A) meson wave functions, (B) spin matrix elements, (C) evaluation of our quark scattering diagrams by inspection, (D) the application of our formalism to systems having identical quarks, and (E) the determination of low-energy meson-meson equivalent potentials near threshold from our Born diagrams.

II. QUARK BORN DIAGRAMS IN MESON-MESON SCATTERING

A. Model Hamiltonian and states

As a first application of the Born diagram formalism we consider scattering of two mesons A and B into final-state mesons C and D. For our discussion we shall refer to a Coulomb-plus-linear potential model with a spin-spin hyperfine term:

$$H = \sum_i -\frac{\hbar^2}{2m_i}\nabla_i^2 + \sum_{i<j} H_{ij} , \qquad (1)$$

$$H_{ij} = \frac{\lambda^a(i)}{2}\frac{\lambda^a(j)}{2}\left\{ +\frac{\alpha_s}{r_{ij}} - \frac{3a}{4}r_{ij} \right.$$

$$\left. -\frac{8\pi\alpha_s}{3m_im_j}\mathbf{S}_i\cdot\mathbf{S}_j\ \delta(\mathbf{r}_{ij}) \right\} . \qquad (2)$$

For antiquarks the color factor $\lambda^a/2$ is as usual replaced by $-\lambda^{aT}/2$. We partition this Hamiltonian H into an $H_0(A,B) = H_0(A)+H_0(B)$ that contains all interactions within each initial meson and an interaction Hamiltonian $H_I(A,B)$, which contains all the remaining terms and describes A-B interactions:

$$H = H_0(A,B) + H_I(A,B) , \qquad (3)$$

$$H_0(A,B) = H_0(A) + H_0(B) . \qquad (4)$$

$H_0(A)$ for example is

$$H_0(A) = \sum_{i\in A} -\frac{\hbar^2}{2m_i}\nabla_i^2 + \sum_{\substack{i<j \\ i,j\in A}} H_{ij} \qquad (5)$$

and $H_I(A,B)$ is

$$H_I(A,B) = \sum_{i\in A, j\in B} H_{ij} . \qquad (6)$$

The initial state $|A,B\rangle$ is by definition an eigenstate of $H_0(A,B)$,

$$H_0(A, B) \, |A, B\rangle = (E_A + E_B) \, |A, B\rangle$$
$$= \left(m_A + \frac{\mathbf{P}_A^{\,2}}{2m_A} + m_B + \frac{\mathbf{P}_B^{\,2}}{2m_B} \right) |A, B\rangle, \tag{7}$$

and the final state $|C, D\rangle$ is an eigenstate of the final-state free Hamiltonian $H_0(C, D)$, which contains all the quark-antiquark interaction terms within mesons C and D:

$$H_0(C, D) \, |C, D\rangle = (E_C + E_D) \, |C, D\rangle$$
$$= \left(m_C + \frac{\mathbf{P}_C^{\,2}}{2m_C} + m_D + \frac{\mathbf{P}_D^{\,2}}{2m_D} \right) |C, D\rangle. \tag{8}$$

$H_0(C, D)$ is defined by analogy with $H_0(A, B)$ above.

The asymptotic $q\bar{q}$ eigenstates of the various H_0 Hamiltonians satisfy Schrödinger equations, which for meson A as an example is

$$H_0(A)|A(\mathbf{P}, \lambda)\,\rangle = E_0(A)|A(\mathbf{P}, \lambda)\,\rangle$$
$$= \left[\sum_{i \in A} -\frac{\hbar^2}{2m_i} \nabla_i^2 + \sum_{\substack{i<j \\ i,j \in A}} \left\{ -\frac{4\alpha_s}{3r_{ij}} + ar_{ij} + \frac{32\pi\alpha_s}{9m_i m_j} \mathbf{S}_i \cdot \mathbf{S}_j \, \tilde{\delta}(\mathbf{r}_{ij}) \right\} \right] |A(\mathbf{P}, \lambda)\,\rangle, \tag{9}$$

where the hyperfine delta function has been suitably regularized. We write the explicit $|A(\mathbf{P}, \lambda)\,\rangle$ state with center-of-mass momentum $\mathbf{P}$ and polarization λ as

$$|A(\mathbf{P}, \lambda)\,\rangle = \sum_{c,\bar{c}=1}^{3} \frac{1}{\sqrt{3}} \, \delta_{c,\bar{c}} \sum_{s,\bar{s}} \iint d^3k \, d^3\bar{k} \, \delta(\mathbf{P} - \mathbf{k} - \bar{\mathbf{k}}) \, \chi_{s\bar{s}}^{(\lambda)} \, \Phi_A(\mathbf{k} - \bar{\mathbf{k}}) \, |q_{\mathbf{k}s}^c\rangle|\bar{q}_{\bar{\mathbf{k}}\bar{s}}^{\bar{c}}\rangle. \tag{10}$$

In this state c and $\bar{c}$ are quark and antiquark color labels and $\{\chi_{s\bar{s}}^{(\lambda)}\}$ is a set of Clebsch-Gordan coefficients appropriate for a spin-S_A meson; as we consider only $L = 0$ mesons, there is no orbital angular momentum to couple to the spin. $\Phi_A(\mathbf{k} - \bar{\mathbf{k}})$ is the $q\bar{q}$ momentum-space wave function, and the delta function $\delta(\mathbf{P} - \mathbf{k} - \bar{\mathbf{k}})$ enforces internal momentum conservation on the meson wave function. These spatial wave functions are discussed in more detail in Appendix A. The dependence of $\Phi_A(\mathbf{k} - \bar{\mathbf{k}})$ on the relative momentum $\mathbf{k} - \bar{\mathbf{k}}$ only and the decoupling of spin and momentum in boosted states result from our use of a nonrelativistic formalism.

We normalize our meson wave functions to

$$\langle \mathbf{P}', \lambda' \, | \, \mathbf{P}, \lambda \,\rangle = \delta_{\lambda\lambda'} \, \delta(\mathbf{P} - \mathbf{P}') \tag{11}$$

and the quarks and antiquarks are defined using Bjorken and Drell conventions [20]:

$$\langle q_{\mathbf{p}',s'}^{c'}|q_{\mathbf{p},s}^c\rangle = \delta^{cc'} \, \delta_{ss'} \, \delta(\mathbf{p} - \mathbf{p}') \tag{12}$$

and

$$|q_{\mathbf{p},s}^c\rangle = b_{\mathbf{p},s}^{c\,\dagger} |0\rangle \tag{13}$$

and similarly for antiquarks. The spin wave functions are normalized to

$$\sum_{ss'} \chi_{ss'}^{(\lambda')\,*} \, \chi_{ss'}^{(\lambda)} = \delta_{\lambda\lambda'}. \tag{14}$$

These constraints in turn imply a normalization for the momentum-space wave function Φ_A, which is

$$\int d^3k \, |\Phi_A(2\mathbf{k} - \mathbf{P})|^2 = 1, \tag{15}$$

independent of $\mathbf{P}$. We may equivalently write a meson state using a composite $q\bar{q}$-meson creation operator, which for meson A is

$$a_{A(\mathbf{P},\lambda)}^{\dagger} = \sum_{c\bar{c}} \sum_{s\bar{s}} \iint d^3k \, d^3\bar{k} \, \frac{1}{\sqrt{3}} \, \delta^{c\bar{c}} \, \chi_{s\bar{s}}^{(\lambda)}$$
$$\times \delta(\mathbf{P} - \mathbf{k} - \bar{\mathbf{k}})$$
$$\times \Phi_A(\mathbf{k} - \bar{\mathbf{k}}) \, b_{\mathbf{k},s}^{c\,\dagger} \, d_{\bar{\mathbf{k}},\bar{s}}^{\bar{c}\,\dagger}. \tag{16}$$

Multimeson states such as the initial $|A, B\rangle$ two-meson state can then be conveniently written as

$$|A, B\,\rangle = a_{A(\mathbf{P}_A,\lambda_A)}^{\dagger} \, a_{B(\mathbf{P}_B,\lambda_B)}^{\dagger} \, |\, 0\,\rangle. \tag{17}$$

B. The "post-prior ambiguity"

In the previous discussion we defined H_0 to be diagonal on the incoming state $|A, B\rangle$; the remaining terms in H by definition constitute H_I. We could of course equivalently define the interaction Hamiltonian H_I using a decomposition in which the final-state mesons C and D are diagonal under an $H_0(C, D)$:

$$H = H_0(C, D) + H_I(C, D), \tag{18}$$

$$H_0(C, D) \, |C, D\rangle = (E_C + E_D) \, |C, D\rangle, \tag{19}$$

$$H_I(C, D) = \sum_{i \in C, j \in D} H_{ij}. \tag{20}$$

This appears to admit an ambiguity; one might expect that the choice of $H_I(C, D)$ in place of $H_I(A, B)$ would lead to a different scattering amplitude at order H_I. This

freedom in the decomposition $H = H_0 + H_I$ is well known in atomic physics, and is known as the "post-prior ambiguity." One may show that the two Born-approximation scattering amplitudes are actually equal [21],

$$\langle C, D| \, H_I(A, B) \, |A, B\rangle = \langle C, D| \, H_I(C, D) \, |A, B\rangle \, , \tag{21}$$

provided that the external states are eigenstates of their respective H_0 free Hamiltonians. If the asymptotic states are instead approximate forms, as in the examples we shall consider here, one generally finds different matrix elements for $H_I(A, B)$ and $H_I(C, D)$. We refer to this as a "post-prior discrepancy." For correct H_0 asymptotic eigenstates, however, these matrix elements are equal, so the choice of decomposition into H_0 and H_I is simply a matter of convention. This result is summarized by equation (43.11) of Schiff [21]. In the following we shall employ the "prior" form $H = H_0(A, B) + H_I(A, B)$ exclusively, so that our interaction describes scattering of A constituents from B constituents. In the $\pi\pi$, KK, and $\rho\rho$ elastic scattering examples we discuss in Section IV this ambiguity is actually not present despite our use of inexact Gaussian wave functions. Reference to the second set of spin matrix elements in Appendix B shows that we would encounter a post-prior ambiguity if we used inexact wave functions in the calculation of $\pi\pi \to \rho\rho$ and $\rho\rho \to \pi\pi$ scattering amplitudes, for example.

C. Scattering amplitudes and matrix elements

At lowest order the scattering process $AB \to CD$ results from the operation of the A-B meson-meson interaction $H_I(A, B)$ on the initial state $|A, B\rangle$: A single operation of $H_I(A, B)$ transforms the $(q\bar{q})_A$ and $(q\bar{q})_B$ pairs from color singlets into color octets; the quark from A and antiquark from B scatter into a color-singlet meson $C = q_A \bar{q}_B$, and the remaining pair $q_B \bar{q}_A$ form a color-singlet meson D. At $O(H_I)$ this rearrangement process alone contributes to meson-meson scattering, since rearrangement is necessary to form color-singlet final states.

The scattering amplitude to leading Born order in H_I is an energy-conserving delta function times the matrix element of H_I between time-independent (Heisenberg picture) states,

$$S_{fi} = \delta_{fi} - 2\pi i \, \delta(E_f - E_i) \, \langle C, D| \, H_I(A, B) \, |A, B\rangle \, , \tag{22}$$

and translational invariance implies that this matrix element may in turn be written as a momentum-space delta function times a state-dependent quantity h_{fi},

$$\langle C, D| \, H_I(A, B) \, |A, B\rangle = \delta(\mathbf{P}_f - \mathbf{P}_i) \, h_{fi} \, , \tag{23}$$

where $\mathbf{P}_i = \mathbf{P}_A + \mathbf{P}_B$ and $\mathbf{P}_f = \mathbf{P}_C + \mathbf{P}_D$. The "physics" of the Born-order scattering amplitude is contained in h_{fi}, and the remainder of the paper is concerned with the calculation of this matrix element and its relation to scattering observables.

Several approaches may be followed in relating the $AB \to CD$ Hamiltonian matrix element h_{fi} to the scat-

tering cross section. A particularly simple approach is to consider $2 \to 2$ scattering of four distinguishable point-like scalars with an interaction Hamiltonian density of $H_I = g\phi_A \phi_B \phi_C \phi_D$. The $O(g)$ S matrix for $AB \to CD$ scattering in the interaction representation is then given by

$$S_{fi} = -i \int_{-\infty}^{\infty} \langle C, D| \, H_I(A, B) \, |A, B\rangle \, dt$$

$$= (2\pi)^4 \, \delta^{(4)}(P_f - P_i) \, \frac{(-ig)}{(2\pi)^6 \sqrt{2E_A \cdots 2E_D}}$$

$$\equiv -2\pi i \, \delta(E_f - E_i) \, \delta(\mathbf{P}_f - \mathbf{P}_i) \, h_{fi} \, . \tag{24}$$

The S matrix is also related to the invariant amplitude $\mathcal{M}_{fi}$ by

$$S_{fi} = \delta_{fi} - i(2\pi)^4 \, \delta^{(4)}(P_f - P_i)$$

$$\times \left\{ \prod_{n=1}^{4} \frac{1}{\sqrt{(2\pi)^3 \, 2E_n}} \right\} \mathcal{M}_{fi} \tag{25}$$

so for this $2 \to 2$ process we conclude that

$$\mathcal{M}_{fi} = \frac{1}{(2\pi)^3} \left\{ \prod_{n=1}^{4} \sqrt{(2\pi)^3 \, 2E_n} \right\} h_{fi} \, . \tag{26}$$

The relation (25) between $\mathcal{M}_{fi}$ and S_{fi} differs from that given by the Particle Data Group [22] in their equation (C1), due to their use of a normalization convention for states (C2) which differs from Bjorken and Drell [20]. Our invariant amplitude $\mathcal{M}_{fi}$ (17) however is identical to the Particle Data Group $\mathcal{M}_{fi}$, so we can use their results for the relation between $\mathcal{M}_{fi}$ and the differential and total cross sections. Specializing to the equal-mass (elastic scattering) case with $M = M_A = M_B = M_C = M_D$, these relations are

$$\left. \frac{d\sigma}{d\Omega} \right|_{c.m.} = \frac{1}{64\pi^2 s} \, |\mathcal{M}_{fi}|^2 = \pi^4 s \, |h_{fi}|^2 \, , \tag{27}$$

$$\frac{d\sigma}{dt} = \frac{1}{16\pi s(s - 4M^2)} \, |\mathcal{M}_{fi}|^2 = \frac{4\pi^5 s}{(s - 4M^2)} \, |h_{fi}|^2 \tag{28}$$

and

$$\sigma = \frac{1}{16\pi s(s - 4M^2)} \int_{-(s-4M^2)}^{0} |\mathcal{M}_{fi}|^2 \, dt$$

$$= \frac{4\pi^5 s}{(s - 4M^2)} \int_{-(s-4M^2)}^{0} |h_{fi}|^2 \, dt \, . \tag{29}$$

The matrix element h_{fi} in these relations is to be evaluated in the c.m. frame.

Finally, an equivalent potential V which gives rise to the same differential cross section near threshold can be found by comparing the Born approximation for equal-mass scattering,

$$\frac{d\sigma}{d\Omega}\bigg|_{c.m.} = |f_{fi}(\Omega)|^2 , \tag{30}$$

$$f_{fi}(\Omega) = -\frac{M}{4\pi} \int d^3x \ V(\mathbf{x}) \ e^{-i\mathbf{q}\cdot\mathbf{x}} , \tag{31}$$

(where $\mathbf{q} = \mathbf{P}_c - \mathbf{P}_A$) to the differential cross section (27). Close to threshold we may take $s = 4M^2$ in (27), which leads to the important result

$$V(\mathbf{x}) = \int d^3q \ h_{fi}(\mathbf{q}) \ e^{i\mathbf{q}\cdot\mathbf{x}} . \tag{32}$$

To generate a $V(r)$ this formalism implicitly assumes that h_{fi} depends on kinematics only through $t = -\mathbf{q}^2$, which is not valid in general; there may be dependence on the Mandelstam variable s as well. This s dependence cannot arise from nonrelativistic scattering through a pure potential, and implies the existence of gradient terms in a more general potential operator $V(\mathbf{x}, \nabla)$; see Barnes and Ghandour [23] and Appendix E for the derivation of such nonlocal potentials from the scattering amplitude.

The relations (27)–(32) between Hamiltonian matrix elements, cross sections, and equivalent potentials may be unfamiliar, so we will demonstrate that they lead to known results in the familiar case of Coulomb scattering. Consider low-energy scattering of distinguishable, equal-mass leptons through a Coulomb potential, with the Hamiltonian

$$H_I = \frac{1}{8\pi} \iint d^3x \ d^3y \ \rho(\mathbf{x}) \ \frac{1}{|\mathbf{x}-\mathbf{y}|} \ \rho(\mathbf{y}) , \tag{33}$$

where

$$\rho(\mathbf{x}) = -e[\psi_{l_1}(\mathbf{x})^\dagger \psi_{l_1}(\mathbf{x}) + \psi_{l_2}(\mathbf{x})^\dagger \psi_{l_2}(\mathbf{x})] . \tag{34}$$

On expanding the fields in creation and annihilation operators and taking the nonrelativistic limit, we find the Hamiltonian matrix element

$$\langle \ l_1(\mathbf{k}'s'), l_2(\mathbf{K}'S')| \ H_I \ | \ l_1(\mathbf{k}s), l_2(\mathbf{K}S)\rangle$$

$$= \frac{\alpha}{\mathbf{q}^2} \frac{u_f^\dagger(l_1)u_i(l_1) \ u_f^\dagger(l_2)u_i(l_2)}{2\pi^2} \delta(\mathbf{k}' + \mathbf{K}' - \mathbf{k} - \mathbf{K})$$

$$\equiv h_{fi} \ \delta(\mathbf{P}_f - \mathbf{P}_i) , \tag{35}$$

so there is only nonflip scattering near threshold, and

$$h_{fi} = \frac{1}{2\pi^2} \frac{\alpha}{\mathbf{q}^2} . \tag{36}$$

Substitution of this h_{fi} into (27) gives the differential cross section

$$\frac{d\sigma}{d\Omega}\bigg|_{c.m.} = \pi^4 s \ |h_{fi}|^2 = \frac{E^2\alpha^2}{\mathbf{q}^4} , \tag{37}$$

which has the nonrelativistic limit

$$\lim_{s\to 4m^2} \frac{d\sigma}{d\Omega}\bigg|_{c.m.} = \frac{m^2\alpha^2}{\mathbf{q}^4} . \tag{38}$$

This is the Rutherford cross section for the scattering of equal-mass distinguishable particles with charge $-e$ and mass m, so we have recovered the correct nonrelativistic result. The potential between leptons which we recover from h_{fi} in the nonrelativistic limit is

$$V(\mathbf{x}) = \int d^3q \ h_{fi}(\mathbf{q}) \ e^{i\mathbf{q}\cdot\mathbf{x}} = \frac{\alpha}{2\pi^2} \int d^3q \ \frac{1}{\mathbf{q}^2} \ e^{i\mathbf{q}\cdot\mathbf{x}} = \frac{\alpha}{r} , \tag{39}$$

which is the Coulomb potential as expected.

III. DETAILED EVALUATION OF QUARK BORN DIAGRAMS

A. Quark diagrams and their component factors

We shall now apply the formalism of the previous section, which relates H_I matrix elements to scattering observables, to the meson-meson scattering problem. There are four Born diagrams which contribute to the $O(H_I)$ scattering amplitude for $AB \to CD$:
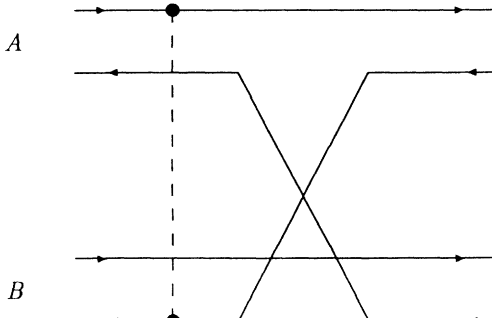
$$\text{capture}_1 = \tag{40}$$

$$\text{capture}_2 = \qquad\qquad\qquad\qquad\qquad\qquad\qquad\qquad\qquad\qquad\qquad\qquad (41)$$

$$\text{transfer}_1 = \qquad\qquad\qquad\qquad\qquad\qquad\qquad\qquad\qquad\qquad\qquad\qquad (42)$$

$$\text{transfer}_2 = \qquad\qquad\qquad\qquad\qquad\qquad\qquad\qquad\qquad\qquad\qquad\qquad (43)$$

In these diagrams the dashed line between fermion lines i and j represents the complete interaction H_{ij} (2), which includes the confining term as well as one-gluon-exchange contributions. In a more general process one would first draw all independent quark line diagrams, and then "decorate" each line diagram with all possible interactions between A constituents and B constituents. In the meson-meson scattering problem we consider, there is only one quark line diagram, and the four independent scattering diagrams result from the four distinct decorations of the line diagram with A-B interactions.

In our meson-meson scattering problem we refer to the first two as "capture" diagrams because the interacting quark-antiquark pair scatter into the same final hadron. In contrast, the quark-quark and antiquark-antiquark interaction diagrams necessarily scatter the interacting constituents into different final hadrons; as the interact-

ing constituents transfer momentum but remain in different hadrons, we call these "transfer" diagrams. We shall see that these sets of diagrams lead to very different momentum dependences, so this is a physically useful categorization.

The h_{fi} matrix element corresponding to each diagram is the product of four factors, which are (1) an overall phase S called the "signature" which arises from the anticommutation of fermion operators, (2) a flavor factor I_{flavor}, (3) a color factor I_{color}, (4) a spin matrix element I_{spin}, and (5) a spatial overlap integral I_{space}:

$$h_{fi} \text{ (particular diagram)} = S I_{\text{flavor}} I_{\text{color}} I_{\text{spin}} I_{\text{space}} . \quad (44)$$

To illustrate the evaluation of these factors we shall consider the contribution of the contact spin-spin hyperfine interaction to the "capture$_1$" diagram in detail, following

which we simply quote results for the other diagrams and for more general interactions.

1. Signature

The "signature" phase $S = \pm 1$ results from the permutation of fermion operators in the scattering matrix element. The operator order in the initial state $\mid A, B \,\rangle$ and the adjoint final state $\langle\, C, D \mid$ is

$$\mid A, B \,\rangle = (b_A^\dagger d_A^\dagger)(b_B^\dagger d_B^\dagger) \mid 0 \rangle, \tag{45}$$

and

$$\langle\, C, D \mid\, = \langle 0 \mid (d_D b_D)(d_C b_C) . \tag{46}$$

Recalling the operator order in H_I, the signature of the

diagram capture$_1$ is

$$S = \text{Phase}\left\{ \langle\, C, D \mid (b_C^\dagger b_A)(d_C^\dagger d_B) \mid A, B \,\rangle \right\}$$

$$= \text{Phase}\left\{ \langle 0 \mid (d_D b_D)(d_C b_C)(b_C^\dagger b_A)(d_C^\dagger d_B) \right.$$

$$\left. \times (b_A^\dagger d_A^\dagger)(b_B^\dagger d_B^\dagger) \mid 0 \rangle \right\} = -1. \tag{47}$$

For a general diagram with our normalization conventions the signature is simply

$$S = (-1)^{N_x} , \tag{48}$$

where N_x is the number of fermion line crossings in the diagram. In our meson-meson scattering problem $N_x = 3$ for all diagrams, so the signature is always -1 (the crossings are indicated in the capture$_1$ diagram below):

$$\text{capture}_1 = \qquad\qquad\qquad\qquad\qquad\qquad\qquad\qquad\qquad\qquad\qquad\qquad (49)$$
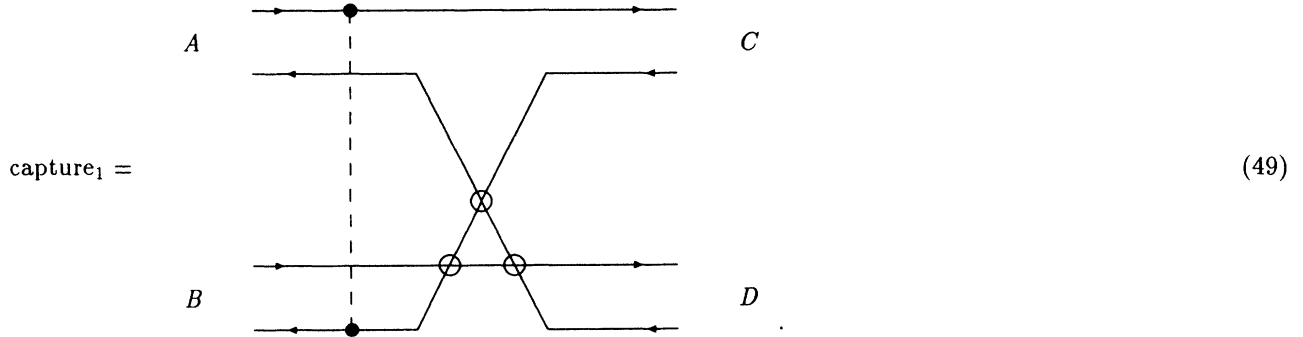
2. Flavor factor

The quark flavor content of the initial and final mesons gives an overall contribution to the scattering amplitude, which can be read directly from the quark line diagram; if the flavor routing specified by the diagram is allowed, the flavor matrix element is unity, otherwise it is zero. Nontrivial contributions to the flavor factor only arise from the external wave functions, which may be superpositions of flavor states such as $(\mid u\bar{u}\rangle - \mid d\bar{d}\rangle)/\sqrt{2}$. In our pedagogical example we assume that the quarks are all distinguishable and the external flavor states all have a positive phase (such as would be the case for $\mid A\rangle = +\mid u\bar{d}\rangle$, $\mid B\rangle = +\mid s\bar{s}\rangle$, $\mid C\rangle = +\mid u\bar{s}\rangle$ and $\mid D\rangle = +\mid s\bar{d}\rangle$). The flavor factor is then simply unity:

$$I_{\text{flavor}} = +1 . \tag{50}$$

Although there is an arbitrariness in the overall phase of states which span an SU(6) multiplet, one should note that their relative phases are fixed by SU(6) symmetry and must be specified consistently, using for example the results of de Swart [24].

3. Color factor

There is also a color factor I_{color} associated with each diagram. For capture$_1$ the color factor can be read from the diagram:

$$I_{\text{color}}(\text{capture}_1) \quad =$$

$$= \frac{\delta_{i\bar{i}}}{\sqrt{3}} \frac{\delta_{j\bar{j}}}{\sqrt{3}} \left\{ \left(\frac{\lambda_{i'i}^a}{2} \right) \delta_{\bar{i}\bar{j}}{}' \left(\frac{-\lambda_{\bar{i}'\bar{j}}^{a\,T}}{2} \right) \delta_{jj'} \right\} \frac{\delta_{i'\bar{i}'}}{\sqrt{3}} \frac{\delta_{j'\bar{j}'}}{\sqrt{3}}$$

$$= -\frac{1}{36} \text{Tr}(\lambda^a \lambda^a) = -\frac{4}{9} \ . \tag{51}$$

The other capture diagram also has a color factor of $-4/9$, and the transfer diagrams have color factors of $+4/9$. We can now evaluate the spin and space dependence of each diagram in the H_I matrix element (23) without explicit reference to color, since the $(\lambda/2)(\lambda/2)$ color dependence of H_I has been subsumed in I_{color}.

4. Spin factor

As an illustration of the spin factor we again consider the diagram "capture$_1$," which is one matrix element of the spin-spin hyperfine interaction Hamiltonian with the $(\lambda/2)(\lambda/2)$ color factor suppressed,

$$H_I = -\frac{8\pi\alpha_s}{3m_q^2} \sum_{\substack{i \in A \\ j \in B}} \mathbf{S}_i \cdot \mathbf{S}_j \ \delta(\mathbf{r}_{ij}) \ . \tag{52}$$

This Hamiltonian can be written as a local nonrelativistic current-current interaction,

$$H_I = -\frac{1}{2} \frac{8\pi\alpha_s}{3m_q^2} \int d^3x \ \mathbf{i}(\mathbf{x}) \cdot \mathbf{i}(\mathbf{x}) \tag{53}$$

where the spin current $\mathbf{i}(\mathbf{x})$ is

$$\mathbf{i}(\mathbf{x}) = \sum_{ss'} \iint \frac{d^3p \, d^3p'}{(2\pi)^3} \left\{ \mathbf{S}_{s's}^{(q)} \, b_{\mathbf{p}',s'}^\dagger b_{\mathbf{p},s} + \mathbf{S}_{s's}^{(\bar{q})} \, d_{\mathbf{p}',s'}^\dagger d_{\mathbf{p},s} \right\} e^{i(\mathbf{p}-\mathbf{p}')\cdot\mathbf{x}} \ . \tag{54}$$

The term which leads to the diagram "capture$_1$" is

$$H_I = -\frac{8\pi\alpha_s}{3m_q^2} \sum_{ss'\bar{s}\bar{s}'} \mathbf{S}(q) \cdot \mathbf{S}(\bar{q}) \iiiint \frac{d^3p \, d^3p' \, d^3\bar{p} \, d^3\bar{p}'}{(2\pi)^3} \ \delta(\mathbf{p}' + \bar{\mathbf{p}}' - \mathbf{p} - \bar{\mathbf{p}}) \ b_{\mathbf{p}',s'}^\dagger b_{\mathbf{p},s} \, d_{\bar{\mathbf{p}}',\bar{s}'}^\dagger d_{\bar{\mathbf{p}},\bar{s}} \ . \tag{55}$$

The explicit initial and final states are given by the analogues of (10) with the flavor and color degrees of freedom suppressed. For example, the initial state is

$$|A, B\rangle = \sum_{s_a \bar{s}_a s_b \bar{s}_b} \iiiint d^3a \, d^3\bar{a} \, d^3b \, d^3\bar{b} \ \delta(\mathbf{A} - \mathbf{a} - \bar{\mathbf{a}}) \ \delta(\mathbf{B} - \mathbf{b} - \bar{\mathbf{b}})$$

$$\times \chi_{s_a \bar{s}_a}^{(\lambda_A)} \chi_{s_b \bar{s}_b}^{(\lambda_B)} \ \Phi_A(\mathbf{a} - \bar{\mathbf{a}}) \ \Phi_B(\mathbf{b} - \bar{\mathbf{b}}) \ |q_{a s_a}^{(A)}\rangle \ |\bar{q}_{\bar{a} \bar{s}_a}^{(A)}\rangle |q_{b s_b}^{(B)}\rangle \ |\bar{q}_{\bar{b} \bar{s}_b}^{(B)}\rangle \ . \tag{56}$$

An expression for the spin factor I_{spin}, which in this case is the matrix element of $\mathbf{S}_i \cdot \mathbf{S}_j$, can be written from the appropriate diagram by inspection. For the diagram capture$_1$ the spin factor is

$$I_{\text{spin}} = \chi_{s_c \bar{s}_c}^{(\lambda_C)*} \chi_{s_d \bar{s}_d}^{(\lambda_D)*} \left\{ \langle s_{\bar{c}} | \mathbf{S} | s_{\bar{b}} \rangle \cdot \langle s_c | \mathbf{S} | s_a \rangle \delta_{s_a s_d} \, \delta_{s_b s_d} \right\} \chi_{s_a \bar{s}_a}^{(\lambda_A)} \chi_{s_b \bar{s}_b}^{(\lambda_B)} \ . \tag{57}$$

This matrix element will in general depend on the spins $S_A \cdots S_D$ and the magnetic quantum numbers $\lambda_A \cdots \lambda_D$ of the external mesons. Since the two-meson scattering amplitudes are usefully described in terms of the spins of the mesons and the total spin of the meson pair, we combine S_A and S_B to form a state with $S_{\text{tot}} = S_{AB} = S_{CD}$; this S_{tot} must also be specified to determine I_{spin}. For our example we specialize to the scattering of two vector mesons in an $S_{\text{tot}} = 2$ state, and on taking $\lambda_{\text{tot}}(= \lambda_A + \lambda_B = \lambda_C + \lambda_D) = +2$, the spin matrix element (57) is found to be

$$I_{\text{spin}}(S_{\text{tot}}, S_A, S_B, S_C, S_D) = I_{\text{spin}}(2, 1, 1, 1, 1) = \left(\langle 11 \mid \tfrac{1}{2}\tfrac{1}{2}, \tfrac{1}{2}\tfrac{1}{2} \; \rangle \right)^4 \langle \uparrow \mid \mathbf{S} \mid \uparrow \rangle \cdot \langle \uparrow \mid \mathbf{S} \mid \uparrow \rangle = 1/4 \ . \tag{58}$$

Values of $I_{\text{spin}}(S_{\text{tot}}, S_A, S_B, S_C, S_D)$ for other spins and the spin matrix elements for the other operators and diagrams are given in Appendix B.

5. Space factor

Finally we require the spatial matrix element I_{space}. To evaluate this we begin by recalling the appropriate four-fermion operator in H_I (53) without spin, flavor, or color degrees of freedom, and derive its matrix element between two-meson states. We then restore the momentum integrations to determine the matrix element of H_I. The capture$_1$ H_I matrix element involves the operator

$$\langle C, D \mid b_{q'}^\dagger b_q \, d_{\bar{Q}'}^\dagger d_{\bar{Q}} \mid A, B \rangle$$

$$= \iiiint d^3c \, d^3\bar{c} \, d^3d \, d^3\bar{d} \ \delta(C - c - \bar{c}) \ \delta(D - d - \bar{d}) \ \Phi_C^*(c - \bar{c}) \ \Phi_D^*(d - \bar{d})$$

$$\times \iiiint d^3a \, d^3\bar{a} \, d^3b \, d^3\bar{b} \ \delta(A - a - \bar{a}) \ \delta(B - b - \bar{b}) \ \Phi_A(a - \bar{a}) \ \Phi_B(b - \bar{b})$$

$$\times \langle c, \bar{c}, d, \bar{d} \mid b_{q'}^\dagger b_q \, d_{\bar{Q}'}^\dagger d_{\bar{Q}} \mid a, \bar{a}, b, \bar{b} \rangle \ . \tag{59}$$

(In this and the following expressions we have suppressed all except spatial degrees of freedom, and have deleted three-vector momentum arrows, which are understood.) The "unscattered" lines $\bar{a} \rightarrow \bar{d}$ and $b \rightarrow d$ in the capture$_1$ diagram give matrix elements of $\langle \bar{d}|\bar{a} \rangle = \delta(\bar{a} - \bar{d})$ and $\langle d|b \rangle = \delta(b - d)$, so the quark matrix element above is

$$\langle c, \bar{c}, d, \bar{d} \mid b_{q'}^\dagger b_q \, d_{\bar{Q}'}^\dagger d_{\bar{Q}} \mid a, \bar{a}, b, \bar{b} \rangle = (-1)\delta(\bar{a} - \bar{d}) \ \delta(b - d) \ \delta(a - q) \ \delta(\bar{b} - \bar{Q}) \ \delta(c - q') \ \delta(\bar{c} - \bar{Q}') \ . \tag{60}$$

The overall phase of (-1) in this matrix element is due to fermion operator permutations, and is the "signature" phase we discussed previously. We choose to treat this phase as a separate factor, so we divide it out of the definition of the "space factor" and will restore it subsequently when we construct the full h_{fi}.

After attaching the external momentum space wave functions and the associated momentum integrations, we use these delta functions to evaluate eight of the momentum integrals in (59). For the capture$_1$ term this gives

$$\langle C, D \mid b_{q'}^\dagger b_q \, d_{\bar{Q}'}^\dagger d_{\bar{Q}} \mid A, B \rangle / S \; = \delta(C - q' - \bar{Q}') \, \delta(A + B - D - q - \bar{Q})$$

$$\times \Phi_C^*(q' - \bar{Q}') \ \Phi_D^*(B - A - \bar{Q} + q) \ \Phi_A(2q - A) \ \Phi_B(B - 2\bar{Q}) \ . \tag{61}$$

This result is then used to construct the full spatial matrix element of H_I, which is

$$\langle C, D \mid H_I \mid A, B \rangle / S$$

$$= -\frac{1}{(2\pi)^3} \frac{8\pi\alpha_s}{3m_q^2} \iiiint d^3q \, d^3q' \, d^3\bar{Q} \, d^3\bar{Q}' \ \delta(q' + \bar{Q}' - q - \bar{Q}) \ \delta(C - q' - \bar{Q}')$$

$$\times \delta(A + B - D - q - \bar{Q}) \ \Phi_C^*(q' - \bar{Q}') \ \Phi_D^*(B - A - \bar{Q} + q)$$

$$\times \Phi_A(2q - A) \ \Phi_B(B - 2\bar{Q}) \ . \tag{62}$$

By inspection, $-q - \bar{Q}$ in the third delta function is constrained to equal $-C$ by the first two delta functions, so the third delta function actually gives external three-momentum conservation and may be removed from the internal integrations:

$$\langle C, D \,|H_I|\, A, B \,\rangle/S = -\frac{1}{(2\pi)^3} \frac{8\pi\alpha_s}{3m_q^2} \delta(C + D - A - B)$$

$$\times \iiiint d^3q \, d^3q' \, d^3\bar{Q} \, d^3\bar{Q}' \, \delta(q' + \bar{Q}' - q - \bar{Q}) \, \delta(C - q' - \bar{Q}')$$

$$\times \Phi_C^*(q' - \bar{Q}') \, \Phi_D^*(B - A - \bar{Q} + q) \, \Phi_A(2q - A) \, \Phi_B(B - 2\bar{Q})$$

$$\equiv I_{\text{space}} \, \delta(P_f - P_i) \,. \tag{63}$$

On carrying out the remaining delta-function integrations we find

$$I_{\text{space}} = -\frac{1}{(2\pi)^3} \frac{8\pi\alpha_s}{3m_q^2} \int d^3q' \, \Phi_C^*(2q' - C) \int d^3q \, \Phi_D^*(2q - A + B - C) \, \Phi_A(2q - A) \, \Phi_B(2q + B - 2C) \,. \tag{64}$$

After translation we recognize the first integral as $(2\pi)^{3/2}$ times the coordinate-space wave function of meson C at contact (see Appendix A). We can also simplify the second integral, because $\mathbf{B} = -\mathbf{A}$ in the c.m. frame in which h_{fi} is to be evaluated. We also translate its variable of integration, which leads to our final result for the spatial factor of the diagram capture$_1$:

$$I_{\text{space}} = -\frac{8\pi\alpha_s}{3m_q^2} \frac{\Psi_C^*(0)}{(2\pi)^{3/2}} \int d^3k \, \Phi_D^*(2k - A) \, \Phi_A(2k + C) \, \Phi_B(2k - C) \,. \tag{65}$$

As this derivation appears somewhat complicated, in Appendix C we give rules which allow one to read this result directly from the scattering diagram.

6. Full h_{fi} for the diagram capture$_1$

On combining the signature, flavor, color, spin, and space factors, we obtain the full h_{fi} matrix element of the diagram capture$_1$:

$$h_{fi}(\text{capture}_1) = S \, I_{\text{flavor}} \, I_{\text{color}} \, I_{\text{spin}} \, I_{\text{space}} = (-1) \times (+1) \times (-4/9) \times (1/4) \times I_{\text{space}}$$

$$= -\frac{8\pi\alpha_s}{27m_q^2} \frac{\Psi_C^*(0)}{(2\pi)^{3/2}} \int d^3k \, \Phi_D^*(2k - A) \, \Phi_A(2k + C) \, \Phi_B(2k - C) \,. \tag{66}$$

B. Total meson-meson Born amplitude and Gaussian approximate wave functions

The remaining three diagrams may be evaluated using essentially identical techniques. The "capture$_2$" diagram gives a result quite similar to that found for "capture$_1$," but instead involves the wave function of final meson D at contact:

$$h_{fi}(\text{capture}_2)$$

$$= -\frac{8\pi\alpha_s}{27m_q^2} \frac{\Psi_D^*(0)}{(2\pi)^{3/2}} \int d^3k \, \Phi_C^*(2k + A) \, \Phi_A(2k + C)$$

$$\times \Phi_B(2k - C) \,. \tag{67}$$

The two "transfer" diagrams lead to a different type of matrix element; since the scattered constituents do not recoil into the same final meson, the overlap integrals no longer lead to a final wave function at contact. The scattering amplitude is instead the product of two two-wave-function overlap integrals, which are "bend factors" that describe the wave-function suppression of unscattered quark lines. There is also a difference in the transfer-diagram color factors, which are $+4/9$ rather than $-4/9$. The transfer diagram matrix elements are explicitly

$$h_{fi}(\text{transfer}_1) = (-1) \times (+1) \times (+4/9) \times (1/4) \times I_{\text{space}}$$

$$= +\frac{8\pi\alpha_s}{27m_q^2} \frac{1}{(2\pi)^3}$$

$$\times \int d^3k \, \Phi_D^*(2k - A) \, \Phi_A(2k + C)$$

$$\times \int d^3k' \, \Phi_C^*(2k' + A) \, \Phi_B(2k' - C) \tag{68}$$

and

$$h_{fi}(\text{transfer}_2) = +\frac{8\pi\alpha_s}{27m_q^2} \frac{1}{(2\pi)^3}$$

$$\times \int d^3k \, \Phi_C^*(2k - C) \, \Phi_A(2k - A)$$

$$\times \int d^3k' \, \Phi_D^*(2k' + C) \, \Phi_B(2k' + A) \,. \tag{69}$$

The sum of the four terms (66)–(69) is the full Born matrix element of the spin-spin Hamiltonian in (2). A complete Born calculation will also require evaluation of the noncontact terms in (2), which we discuss in Section III D, and an evaluation of the overlap integrals (66)–(69), which will evidently only be feasible numerically.

As this paper is largely pedagogical, we shall evaluate the scattering overlap integrals in (66)–(69) analytically using Gaussian wave functions for illustration. One should note that this assumption of asymptotic wave functions which are not H_0 eigenstates can lead to a post-prior discrepancy in general, although there is no such discrepancy in this reaction or in the other cases discussed in detail in this paper. (Reference to Appendix B shows that post-prior ambiguities would be present if we used approximate wave functions in evaluating the "capture" contributions to the processes $PP \to VV$ and $VV \to PP$, for example.) Of course approximate wave functions only give approximate results for the predicted cross sections; a numerical evaluation of these matrix elements and cross sections with more realistic wave functions will appear in a subsequent publication. For our Gaussian example we assume identical wave functions for each of the four external mesons, with the parametrization (see Appendix A)

$$\Phi(\mathbf{k} - \bar{\mathbf{k}}) = \sqrt{8}\left(\frac{\lambda}{\pi}\right)^{3/4} \exp\left\{-\frac{\lambda}{2}\left(\mathbf{k} - \bar{\mathbf{k}}\right)^2\right\} . \quad (70)$$

The overlap integrals (66)–(69) are straightforward, and lead to the following matrix elements (which we give as functions of Mandelstam variables):

$h_{fi}(\text{capture}_1)$

$$= h_{fi}(\text{capture}_2)$$
$$= -\frac{8\pi\alpha_s}{27m_q^2}\frac{1}{(2\pi)^3}\frac{8}{3\sqrt{3}}\exp\left\{-\frac{\lambda(s - 4M^2)}{3}\right\} , \quad (71)$$

$$h_{fi}(\text{transfer}_1) = +\frac{8\pi\alpha_s}{27m_q^2}\frac{1}{(2\pi)^3}\exp\left\{\frac{\lambda u}{2}\right\} \quad (72)$$

and

$$h_{fi}(\text{transfer}_2) = +\frac{8\pi\alpha_s}{27m_q^2}\frac{1}{(2\pi)^3}\exp\left\{\frac{\lambda t}{2}\right\} . \quad (73)$$

The total Born matrix element with Gaussian wave functions can thus be written compactly as

$h_{fi}(\text{Born})$

$$= +\frac{8\pi\alpha_s}{27m_q^2}\frac{1}{(2\pi)^3}\left[\exp\left\{\frac{\lambda t}{2}\right\} + \exp\left\{\frac{\lambda u}{2}\right\}\right.$$
$$\left. -\frac{16}{3\sqrt{3}}\exp\left\{-\frac{\lambda(s - 4M^2)}{3}\right\}\right] . \quad (74)$$

Note that the capture diagrams are purely S wave in this approximation, whereas the transfer diagrams lead to strong angular dependence. Although the pure S wave result is an artifact of the Gaussian wave functions and the delta-function interaction, it should nonetheless be possible to distinguish the contributions of the different diagrams experimentally from their distinct angular dependences. To complete the calculation of differential and total cross sections we must substitute (74) into the relations (28) and (29); this we defer to the next section, in which we discuss $\pi\pi$ and KK scattering and compare our predictions to experiment.

C. Coulomb and linear potential contributions

Thus far we have only given detailed results for scattering through the spin-spin color-hyperfine contact interaction. This is in part because the contact interaction leads to a particularly simple product form for the scattering amplitudes, which can be evaluated in closed form given Gaussian $q\bar{q}$ wave functions. Another justification for concentrating on the spin-spin contact term is that the noncontact terms (color Coulomb and the linear confining term) are numerically unimportant in the pseudoscalar-pseudoscalar channel [25]. In other channels such as vector-vector, however, this is found not to be the case, and the noncontact interactions give important contributions. We will evaluate these contributions numerically in future work; for the present we simply cite the results we find when we generalize our four spatial matrix elements to a noncontact interaction. These are

$$I_{\text{space}}(\text{capture}_1) = \iint d^3a\, d^3c\, \Phi_A(2\mathbf{a} - \mathbf{A})\, \Phi_B(2\mathbf{a} - \mathbf{A} - 2\mathbf{C})\, V(|\mathbf{a} - \mathbf{c}|)\, \Phi_C^*(2\mathbf{c} - \mathbf{C})\, \Phi_D^*(2\mathbf{a} - 2\mathbf{A} - \mathbf{C}) , \quad (75)$$

$$I_{\text{space}}(\text{capture}_2) = \iint d^3a\, d^3d\, \Phi_A(2\mathbf{a} - \mathbf{A})\, \Phi_B(2\mathbf{a} - \mathbf{A} - 2\mathbf{C})\, V(|\mathbf{a} - \mathbf{d} - \mathbf{A} - \mathbf{C}|)\, \Phi_C^*(2\mathbf{a} - \mathbf{C})\, \Phi_D^*(2\mathbf{d} + \mathbf{C}) , \quad (76)$$

$$I_{\text{space}}(\text{transfer}_1) = \iint d^3a\, d^3b\, \Phi_A(2\mathbf{a} - \mathbf{A})\, \Phi_B(2\mathbf{b} + \mathbf{A})\, V(|\mathbf{a} - \mathbf{b} - \mathbf{A} - \mathbf{C}|)\, \Phi_C^*(2\mathbf{b} + 2\mathbf{A} + \mathbf{C})\, \Phi_D^*(2\mathbf{a} - 2\mathbf{A} - \mathbf{C}) , \quad (77)$$

and

$$I_{\text{space}}(\text{transfer}_2) = \iint d^3a\, d^3b\, \Phi_A(2\mathbf{a} - \mathbf{A})\, \Phi_B(2\mathbf{b} + \mathbf{A})\, V(|\mathbf{a} - \mathbf{b} - \mathbf{A} - \mathbf{C}|)\, \Phi_C^*(2\mathbf{a} - \mathbf{C})\, \Phi_D^*(2\mathbf{b} + \mathbf{C}) , \quad (78)$$

where $V(|\mathbf{p}|)$ is the Fourier transform of the spatial interaction,

$$V(|\mathbf{p}|) = \frac{1}{(2\pi)^3} \int d^3x\, e^{i\mathbf{p}\cdot\mathbf{x}} v(r) \ . \tag{79}$$

As an example of the application of these formulas, the spin-spin contact interaction corresponds to

$$v(r) = -\frac{8\pi\alpha_s}{3m_q^2}\, \delta(\mathbf{x}) \ , \tag{80}$$

for which $V(|\mathbf{p}|)$ is

$$V(|\mathbf{p}|) = -\frac{1}{(2\pi)^3}\frac{8\pi\alpha_s}{3m_q^2} \ . \tag{81}$$

On substituting this V into (75)–(78) and replacing the signature, spin, and color factors, we recover the contact spin-spin matrix elements (66)–(69).

For a long-range interaction such as the linear confining term these spatial overlap integrals are individually infrared divergent, and these infrared-divergent parts cancel when we construct color-singlet scattering amplitudes. For this reason it will be appropriate in a numerical study to evaluate a complete color-singlet amplitude. Singlet amplitudes are sums of the four spatial matrix elements (75)–(78) with appropriate color coefficients. The color Coulomb interaction itself gives the interaction

$$V(|\mathbf{p}|) = -\frac{\alpha_s}{2\pi^2}\frac{1}{\mathbf{p}^2} \ ; \tag{82}$$

evidently the corresponding Coulomb integrals (75)–(78) should also be evaluated carefully near $\mathbf{p}^2 = 0$.

IV. APPLICATION TO $\pi^+\pi^+$ AND K^+K^+ SCATTERING

The matrix element (74) for the scattering of distinguishable S wave $q\bar{q}$ vector mesons in the $S_{\text{tot}} = 2$ channel was derived in the previous section as a pedagogical example. A more familiar channel, for which experimental data exists, is $I = 2$ $\pi\pi$ elastic scattering; the corresponding Hamiltonian matrix element can be obtained from (74) in the Gaussian-wave-function approximation after a few minor modifications. We will also briefly consider $I = 1$ KK scattering, as this channel leads to the same analytic results. First, as discussed in Appendix D, the presence of identical quarks and antiquarks leads to additional scattering diagrams that symmetrize the scattering amplitude in t and u; since the scattering amplitude for a contact interaction happens to be symmetric in t and u for distinguishable quarks, the contribution of the new diagrams equals the previous h_{fi}, so the net effect of having identical quarks and antiquarks is simply to multiply h_{fi} by a factor of 2. Second, the spin factors for pseudoscalar-pseudoscalar scattering in S wave are $-3/8$ and $+3/8$ for "capture" and "transfer" diagrams respectively, whereas for $S_{\text{tot}} = 2$ vector-vector scattering they were both $+1/4$. The flavor and color factors are unchanged. These modifications lead to the $I = 2$ $\pi\pi$ "$\pi^+\pi^+$" and $I = 1$ KK "K^+K^+" scattering amplitude

$$h_{fi}(\text{Born}) = +\frac{8\pi\alpha_s}{9m_q^2}\frac{1}{(2\pi)^3}\left[\exp\left\{\frac{\lambda t}{2}\right\} + \exp\left\{\frac{\lambda u}{2}\right\}\right.$$
$$\left. +\frac{16}{3\sqrt{3}}\exp\left\{-\frac{\lambda\xi}{3}\right\}\right] \ . \tag{83}$$

where $\xi = s - 4M^2$. One may use this full hyperfine Born h_{fi} and the relations (28)–(29) to obtain the differential and total cross sections in closed form in the Gaussian-wave-function approximation. The differential cross section is

$$\frac{d\sigma}{dt} = \frac{4\pi\alpha_s^2 s}{81\lambda\xi}\left[\exp\left\{\frac{\lambda t}{2}\right\} + \exp\left\{\frac{\lambda u}{2}\right\}\right.$$
$$\left. +\frac{16}{3\sqrt{3}}\exp\left\{-\frac{\lambda\xi}{3}\right\}\right]^2 \ . \tag{84}$$

On integrating this over t and multiplying by $1/2$ for identical final-state mesons, we find the total identical pseudoscalar-pseudoscalar ($\pi^+\pi^+$ or K^+K^+) cross section,

$$\sigma = \frac{4\pi\alpha_s^2 s}{81m_q^4}\left[\frac{128}{27}e^{-2\lambda\xi/3} + \frac{64}{3\sqrt{3}}\frac{e^{-\lambda\xi/3}(1 - e^{-\lambda\xi/2})}{\lambda\xi}\right.$$
$$\left. +\frac{1 - e^{-\lambda\xi}}{\lambda\xi} + e^{-\lambda\xi/2}\right] \ . \tag{85}$$

In this expression the first contribution comes from the transfer diagrams squared, the second from transfer-capture interference, and the final two are from the capture diagrams. This cross section is shown in Figure 1 with parameters appropriate for $I = 2$ $\pi\pi$ scattering; we have taken $M = 0.138$ GeV, $\alpha_s = 0.6, m_q = 0.33$ GeV and $\beta_{\text{SHO}} = 0.337$ GeV, corresponding to $\lambda = 2.20$ GeV^{-2}. The values of α_s and m_q are conventional for light quarks, and β_{SHO} is taken from a fit to the S-wave phase shift which we shall describe subsequently.

This cross section approaches a threshold limit of
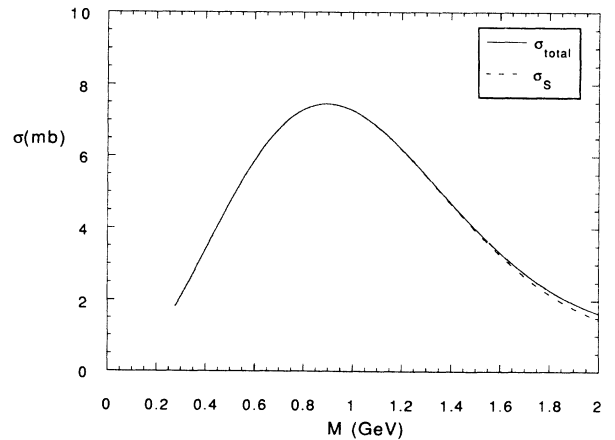
FIG. 1. Total and S-wave $I = 2$ $\pi\pi$ cross sections ($\alpha_s = 0.6$, $m_q = 0.33$ GeV and fitted parameter $\beta_{\text{SHO}} = 0.337$ GeV.

$$\lim_{s \to 4M^2} \sigma = \sigma_0 = \frac{32(91 + 48\sqrt{3})}{2187} \frac{\pi \alpha_s^2 M^2}{m_q^4} , \qquad (86)$$

which with our $\pi\pi$ parameters is 1.8 mb. This limit is conventionally expressed as an $I = 2$ $\pi\pi$ scattering length a_2, defined by

$$\lim_{s \to 4M^2} \sigma = 8\pi a_2^2 . \qquad (87)$$

Comparison of these results gives our prediction for the S-wave $I = 2$ scattering length:

$$a_2 = -\frac{2}{9}\left(1 + \frac{8}{3\sqrt{3}}\right)\frac{\alpha_s M}{m_q^2} . \qquad (88)$$

[We have also restored the negative sign characteristic of a repulsive interaction, which is implicit in the positive h_{fi} matrix element (83).] For our parameters $M = 0.138$ GeV, $\alpha_s = 0.6$ and $m_q = 0.33$ GeV this is

$$\frac{a_2}{M^{-1}} = -0.059 . \qquad (89)$$

This is clearly in satisfactory agreement with Weinberg [2] as well as the more recent parametrization of Morgan and Pennington [26]; both find

$$\frac{a_2}{M^{-1}} = -0.06 . \qquad (90)$$

In this low-energy limit our theoretical cross section is dominated by the capture diagrams and the capture-transfer interference terms; since interference is important, the relative phases and strengths of these diagrams determine which channels have large scattering amplitudes near threshold. The pseudoscalar-pseudoscalar system has a large threshold scattering amplitude because the capture and transfer diagrams have the same phase in this spin state. As an illustration of the importance of relative phases, if these phases were opposite (as is the case in $S_{tot} = 2$ vector-vector scattering) the pseudoscalar-pseudoscalar Born cross section at threshold would be suppressed by a factor of $(91 - 48\sqrt{3})/(91 + 48\sqrt{3}) \approx 0.045$, which is more than an order of magnitude.

To compare with the experimental S-wave phase shift above threshold we separate the S-wave part of our predicted $I = 2$ $\pi\pi$ cross section (85) by integrating h_{fi} (83) over angles; this gives

$$\sigma_S = \frac{32\pi\alpha_s^2 s}{81 m_q^4 \lambda^2 \xi^2}\left[1 - e^{-\lambda\xi/2} + \frac{4\lambda\xi}{3\sqrt{3}}e^{-\lambda\xi/3}\right]^2 . \qquad (91)$$

The S-wave $I = 2$ $\pi\pi$ cross section (91) and the full cross section (85) are shown from threshold to $M_{\pi\pi} = 2.0$ GeV in Figure 1; their near equality below 1.5 GeV shows that the predicted cross section is dominantly S wave over this energy range, as is observed experimentally [27]. The S wave $I = 2$ $\pi\pi$ phase shift $\delta_2^{(\ell=0)}$ is related to (85) by

$$\sigma_S = \frac{8\pi}{\mathbf{k}^2}\sin^2\delta_2^{(0)} , \qquad (92)$$

which gives

$$\sin\delta_2^{(0)} = -\left\{\frac{\alpha_s}{9\lambda m_q^2}\sqrt{\frac{s}{\xi}}\left(1 - e^{-\lambda\xi/2} + \frac{4\lambda\xi}{3\sqrt{3}}e^{-\lambda\xi/3}\right)\right\} . \qquad (93)$$

Although we use (92) to define the magnitude of our phase shift, one might instead equate our purely real Born amplitude to the leading term in $[\exp(2i\delta) - 1]/2i$, so that (93) and (94) would be expressions for $\delta_2^{(\ell)}$ rather than $\sin\delta_2^{(\ell)}$. For the phase shifts we consider here the difference between δ and $\sin\delta$ is not particularly important numerically.

We show this predicted $\sin\delta_2^{(0)}$ (93) in Figure 2 from threshold to $M_{\pi\pi} = 1.5$ GeV, together with the data of Hoogland et al. [27]. (In a recent review Ochs [28] noted that this experiment, with 4.5×10^4 events, had the best statistics of previous $\pi\pi$ studies, so we shall use the two sets of phase shifts quoted by Hoogland et al. as our experimental values.) The agreement between our prediction (93) and the data in Figure 2 is evidently very good. The theoretical curve is for $M = 0.138$ GeV, $\alpha_s/m_q^2 = 0.6/(0.33 \text{ GeV})^2 = 5.51$ GeV^{-2} (from quark-model phenomenology) and uses a fitted value of $\beta_{\text{SHO}} = 1/2\sqrt{\lambda} = 0.337$ GeV. The fitted β_{SHO} is reassuringly close to the standard quark-model value of $\beta_{\text{SHO}} = 0.3$ GeV. This β_{SHO} is the averages of fits to the "method A" and "method B" data sets of Hoogland et al., which gave very similar values. (In fitting the data we minimized the linear moduli $\sum_i |\delta^i(\text{theor}) - \delta^i(\text{expt})|$ rather than their squares.) We chose to fix α_s and m_q at conventional values because the optimum parameter set $(\alpha_s/m_q^2, \beta_{\text{SHO}}) = (4.48 \text{ GeV}^{-2}, 0.385 \text{ GeV})$ differed little from the conventional $\alpha_s/m_q^2 = 5.51$ GeV^{-2}, and the two sets gave similar predictions for the S-wave phase shift. Since β_{SHO} is less well established in quark model phenomenology we fitted this parameter to the data. It would be very useful to extend the experimental measurements of $I = 2$ $\pi\pi$ scattering to higher energies to test the predicted phase shift, which has an extremum near 1.5 GeV; this is the highest energy for which there have been accurate measurements, and the data shows no clear evi-
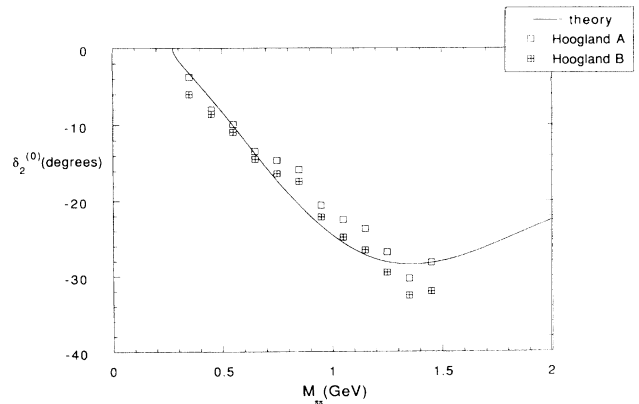
FIG. 2. $I = 2$ $\pi\pi$ S-wave phase shift and the data of Hoogland et al. for $\alpha_s = 0.6$, $m_q = 0.33$ GeV and β_{SHO} (fitted)$=0.337$ GeV.

dence for this behavior. A calculation of the phase shifts with Coulomb-plus-linear wave functions would also be advisable as a test of their sensitivity to the wave functions assumed.

The higher (even-ℓ) partial waves allowed in $I = 2$ $\pi\pi$ scattering are also of interest, since the D-wave phase shift has been measured by Hoogland et al. [27]. This phase shift is quite small; it is smaller than $-1°$ from threshold to $\sqrt{s} = 0.8$ GeV, and has increased to only about $-3°$ at $\sqrt{s} = 1.5$ GeV. We may determine all the partial-wave phase shifts from the Gaussian wave-function matrix element (83) using the integral $\int_{-1}^{1} P_\ell(\mu) e^{a\mu} d\mu = 2i_\ell(a)$, where $i_\ell(x)$ is the modified spherical Bessel function of the first kind. This gives, for ℓ even and ≥ 2

$$\sin \delta_2^{(\ell)} = -\left\{ \frac{\alpha_s}{18m_q^2} \sqrt{s\xi}\, e^{-\lambda\xi/4}\, i_\ell(\lambda\xi/4) \right\}, \qquad (94)$$

with a corresponding contribution to the ℓth partial-wave cross section of

$$\sigma_\ell = (2\ell + 1) \frac{8\pi\alpha_s^2 s}{81m_q^4} e^{-\lambda\xi/2}\, i_\ell(\lambda\xi/4)^2 . \qquad (95)$$

These higher partial waves have several interesting features. The low-energy phase shifts are

$$\delta_2^{(\ell)} \approx -\frac{1}{(2\ell + 1)!!} \frac{2\alpha_s M}{m_q^2} \lambda^\ell |\mathbf{k}|^{2\ell+1} , \qquad (96)$$

which exhibits the $|\mathbf{k}|^{2\ell+1}$ behavior characteristic of potential scattering at low energies. As the invariant mass s is increased the $\ell \geq 2$ phase shifts all fall monotonically, and all (including $\ell = 0$) approach the same negative constant:

$$\lim_{s \to \infty} \delta_2^{(\ell)} = -\arcsin\left(\frac{\alpha_s}{9m_q^2\lambda} \right) \quad (\ell \text{ even}) . \qquad (97)$$

With our fitted parameters this asymptotic angle is a surprisingly large $-16°$, but these large values are predicted at high energies which are presumably beyond the range of validity of the model. The actual values predicted for the D-wave phase shift by

$$\delta_2^{(\ell=2)} = -\arcsin\left\{ \frac{\alpha_s}{18m_q^2} \sqrt{s\xi}\, e^{-\lambda\xi/4}\, i_2(\lambda\xi/4) \right\} \qquad (98)$$

are smaller than the experimental values of Hoogland et al. [27], provided that we use the Gaussian wave-function parameters found in our best fit to the S-wave phase shifts. At $\sqrt{s} = 1.5$ GeV the predicted D-wave phase shift is only about $-0.9°$, whereas experimentally it is about $-3°$. The D-wave is most sensitive to the large-distance parts of the $q\bar{q}$ wave function; a broader wave function gives increased small-angle scattering, and hence supports a larger D-wave phase shift. Although one can obtain a reasonable fit to the D-wave data alone with a broader Gaussian, a single Gaussian does not allow a good fit to both S-wave and D-wave data. It may

be possible to fit both with a Coulomb-plus-linear wave function, which falls more slowly than a Gaussian at large distances. Alternatively, since the D-wave amplitude is very small, it may be dominated by other effects which we have neglected, such as the spin-independent potential or the tensor interaction. We also note that the "capture diagrams" are only pure S-wave in the Gaussian wave-function approximation, and with Coulomb-plus-linear wave functions will make a contribution to the D wave. Clearly it will be an interesting exercise to calculate the phase shifts due to these interactions with Coulomb-plus-linear wave functions.

We have seen that below $\sqrt{s} = 1.5$ GeV (the largest energy for which accurate experimental phase shifts exist) the predicted and observed $\pi\pi$ cross sections are dominantly isotropic, with σ_D/σ_S experimentally $\lesssim 5\%$. For $\sqrt{s}$ much larger than $1/\sqrt{\lambda}$, however, the anisotropic component becomes important, and at large s a strongly peaked differential cross section is predicted. In the small-t/s regime this cross section asymptotically approaches

$$\lim_{s \to \infty} \frac{d\sigma}{dt} = \frac{4\pi\alpha_s^2}{81\lambda} e^{\lambda t} , \qquad (99)$$

which is reminiscent of the e^{bt} "diffractive peak" familiar from experimental studies of hadron scattering at high energies. The exchange of vacuum quantum numbers in t channel often associated with diffractive scattering is also realized here, because the $e^{\lambda t}$ behavior arises from the "transfer diagrams" in which a $u\bar{u}$ or $d\bar{d}$ pair (or $\bar{s}s$ for $K^+ K^+$) cross between hadrons. Of course the exact exponential form is an artifact of our assumption of Gaussian wave functions, but we expect a similar small-t peak from more realistic Coulomb-plus-linear wave functions as well.

Although the similarity of our predictions to diffractive scattering is suggestive, it would be unrealistic to attribute diffraction to these Born-level quark diagrams. There are two obvious problems with such an identification. First, the "transfer" diagrams, which predict a high-energy exponential peak in t, contribute to pp elastic scattering but not to $p\bar{p}$; the approximate equality of these cross sections at high energies is a well-known experimental result [22]. Second, the phase of the forward elastic scattering amplitude in $p\bar{p}$ and pp at high energies has been determined from interference with photon exchange [17], and has relatively strong energy dependence. The Born diagrams of course have an energy-independent phase. The transition region between $\sqrt{s} \lesssim 1.5$ GeV (for which our $I = 2$ $\pi\pi$ quark Born amplitudes are in good agreement with experiment) and $\sqrt{s} \gtrsim 20$ GeV (where the close relation between pp and $p\bar{p}$ scattering becomes apparent) would evidently be the interesting regime in which to study the onset of the diffractive scattering mechanism.

Although our Born diagrams evidently do not reproduce observed diffractive amplitudes, their high energy limit may be of interest nonetheless. As we increase s, most contributions to the Born elastic cross section (85) decrease exponentially, leaving a residual constant

cross section at high energies. This constant contribution arises from the $e^{\lambda t}$ diffractive peak, which is due to the transfer diagrams, and in $\pi^+ \pi^+$ (and $K^+ K^+$) corresponds to vacuum quantum number exchange. The high-energy limit of these cross sections is

$$\lim_{s \to \infty} \sigma = \sigma_\infty = \frac{4\pi\alpha_s^2}{81m_q^4\lambda} = \frac{16\pi\alpha_s^2\beta_{\text{SHO}}^2}{81m_q^4} , \qquad (100)$$

which for our $\pi^+ \pi^+$ parameters is 0.6 mb. The ratio of the high- and low-energy limits in pseudoscalar-pseudoscalar scattering is

$$\sigma_\infty/\sigma_0 = \frac{27}{8(91 + 48\sqrt{3})} \frac{1}{\lambda M^2}$$

$$= \frac{27}{2(91 + 48\sqrt{3})} \left(\frac{\beta_{\text{SHO}}}{M}\right)^2 , \qquad (101)$$

which is approximately 0.34 for $\pi^+\pi^+$ with our parameters. This case is somewhat anomalous, however, because the $I = 2$ $\pi\pi$ cross section is predicted to increase above threshold to a maximum value of about 7 mb near $\sqrt{s} = 0.9$ GeV before decreasing to the high-energy limit.

These formulas also apply to $I = 1$ KK scattering with a change of parameters. We take $M = 0.495$ GeV for the kaon mass and use an intermediate strange-nonstrange quark mass of $m_q = 0.44$ GeV; $\alpha_s = 0.6$ and $\beta_{\text{SHO}} = 0.337$ GeV are left unchanged from the fit to S-wave $\pi\pi$ phase shifts. The predicted $I = 1$ KK cross section and S-wave phase shift are shown in Figure 3 and Figure 4, respectively. The threshold value we find for the K^+K^+ cross section is 7.3 mb, and it monotonically decreases with increasing KK invariant mass. Although there have been no experimental measurements of this cross section, variational techniques have recently been applied to this system by Weinstein [29]. Our S-wave phase shift at moderate energies ($M_{KK} \lesssim 2.0$ GeV) closely resembles the prediction of Weinstein [29] in form, but is only about half as large; this discrepancy may reflect our conclusion that only pion equivalent potentials
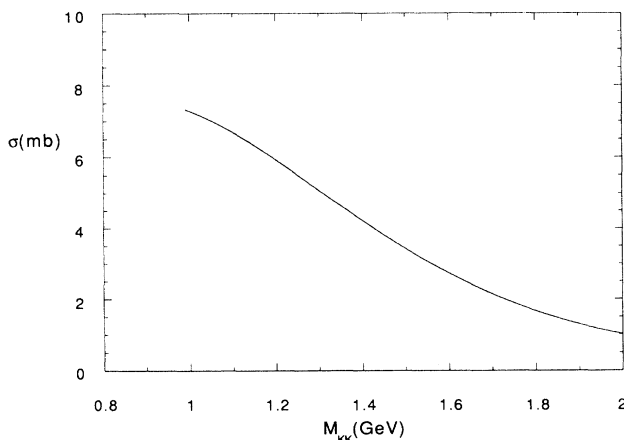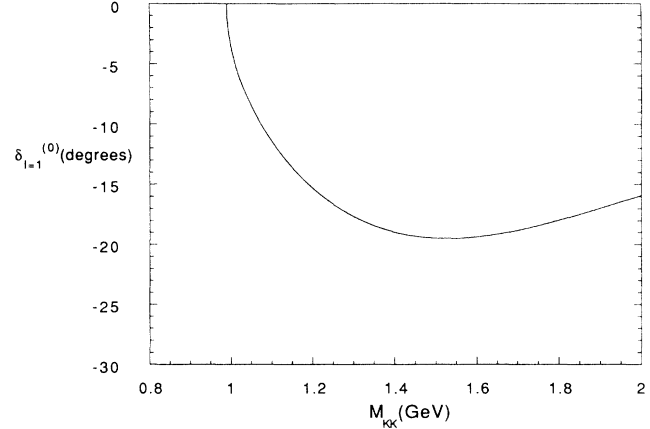
FIG. 4. $I = 1$ KK S-wave phase shift. Parameters $\alpha_s = 0.6$, $m_q = 0.44$ GeV, $\beta_{\text{SHO}} = 0.337$ GeV.

require large rescalings. (Weinstein changed the length and magnitudes scales of his calculated KK potential, for reasons discussed in Appendix E.) At higher energies we find a relatively small limiting value of 0.2 mb for this cross section; the ratio of high- and low-energy limits is $\sigma_\infty/\sigma_0 = 0.026$, approximately an order of magnitude smaller than for $\pi\pi$, since this ratio is predicted to be proportional to $1/M^2$ [Eq. (101)].

The rapid decrease of elastic cross sections from values of ~ 10–100 mb near threshold to a persistent high-energy component of a few mb at $\sqrt{s} \sim 5$–50 GeV is a well-known feature of experimental meson-baryon and baryon-baryon scattering. (See for example the K^+P and PP elastic cross sections in the Particle Data Group compilation [22].) Our results reproduce these general features, albeit with a phase that is not consistent with the observed diffractive amplitude.

We also quote the $S_{\text{tot}} = 2$, $I = 2$ "$\rho^+\rho^+$" S-wave phase shift due to the spin-spin color hyperfine term in the Gaussian wave-function approximation. For vector-vector scattering we actually find dominant contributions from color Coulomb and linear confining terms, which are discussed elsewhere[25]. For this reason these hyperfine results do not accurately model $I = 2$ $\rho\rho$ interactions near threshold, and are only presented as a pedagogical example for comparison with $\pi\pi$ and KK. Although the $\rho^+\rho^+$ cross section is experimentally inaccessible, it may be possible to infer meson-meson interactions in these higher-lying channels from invariant-mass distributions near threshold. This possibility has been discussed by Weinstein [29] for KK systems. The hyperfine contribution to the $^5S_2$ $I = 2$ $\rho\rho$ phase shift is

$$\sin \delta_2^{(0)}(\rho\rho) = -\left\{ \frac{2\alpha_s}{27\lambda m_q^2} \sqrt{\frac{s}{\xi}} \left(1 - e^{-\lambda\xi/2}\right.\right.$$

$$\left.\left. - \frac{4\lambda\xi}{3\sqrt{3}} e^{-\lambda\xi/3}\right)\right\} , \qquad (102)$$

and is much weaker than was the case for pseudoscalar-

FIG. 3. Total $I = 1$ KK cross section for $\alpha_s = 0.6$, $m_q = 0.44$ GeV and $\beta_{\text{SHO}} = 0.337$ GeV.

pseudoscalar scattering, due to destructive capture-transfer interference. Near threshold it corresponds to a $\rho^+\rho^+$ cross section of only about 1.1 mb, and because the capture diagram contribution is largest and is attractive in this channel, one finds a weakly attractive interaction with a positive phase shift near threshold. With increasing $\rho\rho$ invariant mass, the transfer diagrams become dominant, and the effective interaction becomes repulsive. The crossover between these diagrams results in a zero in the S-wave phase shift near 2.0 GeV and a very small, highly anisotropic cross section near this energy. At higher energies the $\rho^+\rho^+$ cross section approaches 4/9 of the K^+K^+ cross section. (This factor is the relative spin matrix element squared.)

Although we have demonstrated that numerically plausible results for pseudoscalar-pseudoscalar scattering follow from these quark Born diagrams, these calculations have used approximate Gaussian wave functions and for this reason are not definitive; they are intended only as illustrations of the method and of approximate results. The actual evaluation of scattering amplitudes will involve numerical integration of correct $q\bar{q}$ wave functions, as well as evaluations of the Coulomb and linear contributions to the scattering amplitude, which will be presented in a subsequent paper. The Coulomb and linear contributions actually are found to be small for the pseudoscalar-pseudoscalar case, but they are important in some vector channels [25] and hence should not be neglected in general.

V. CONCLUSIONS

In this paper we have developed a formalism for calculating hadron-hadron scattering amplitudes in Born approximation given an interquark Hamiltonian and external $q\bar{q}$ wave functions. The relation between the Hamiltonian matrix element and differential and total cross sections and elastic phase shifts was derived, and the generalization of the method to identical quarks was also developed. To simplify the calculation of the underlying Hamiltonian matrix elements we presented our techniques in a diagrammatic formalism, so the scattering amplitudes can be written directly from the Born scattering diagrams.

As an illustration of our techniques we treated elastic $I = 2$ $\pi\pi$ and $I = 1$ KK scattering explicitly, given Gaussian external $q\bar{q}$ wave functions and taking the color-magnetic hyperfine component of one gluon exchange as our scattering Hamiltonian. We derived closed-form Born phase shifts and differential and total cross sections for these reactions. The S-wave $\pi\pi$ phase shift predicted with standard quark model parameters was found to be in good agreement with data over the full range of invariant masses for which accurate experimental measurements exist, $M_{\pi\pi} = 0.3$ to 1.5 GeV. We also showed how meson-meson potentials may be extracted from our Born scattering amplitudes near threshold, and compared our $\pi\pi$ and KK potentials to the results of Weinstein and Isgur. At higher energies our predicted differential cross section showed an exponential peak at small t, due to the contribution of "transfer diagrams"

in which gluon exchange takes place between q-q or $\bar{q}$-$\bar{q}$ in different mesons (but not between q-$\bar{q}$). This t dependence and the net exchange of vacuum quantum numbers are reminiscent of diffractive scattering, although the phase of the Born amplitude precludes identification of these Born diagrams as the mechanism of diffraction. It will be important in future work to test the sensitivity of our results to the external $q\bar{q}$ wave functions and to determine the Born phase shifts and cross sections with more realistic Coulomb-plus-linear wave functions.

Our techniques are immediately applicable to other systems in which $q\bar{q}$ annihilation and s-channel resonances are not important, for example kaon-nucleon scattering [31] (but not antikaon-nucleon) and two-baryon systems. It would be particularly interesting to calculate the nucleon-nucleon interaction using these straightforward Born-diagram techniques, to determine whether the short-distance repulsive core can be obtained in Born approximation. Applications to systems in which annihilation and resonance production is important, such as $I = 0$ $\pi\pi$ and π-nucleon scattering, will require further development of the formalism to allow the incorporation of other sectors of Hilbert space as intermediate states.

ACKNOWLEDGMENTS

APPENDIX A: MESON SPATIAL WAVE FUNCTIONS

The complete state vector of an S-wave $q\bar{q}$ meson with total momentum $\mathbf{P}$ and spin polarization λ can be written nonrelativistically as

$$|\mathbf{P},\lambda\rangle = \sum_{c,\bar{c}=1}^{3} \frac{1}{\sqrt{3}}\delta_{c\bar{c}} \sum_{s,\bar{s}} \iint d^3x\, d^3\bar{x}\; \chi_{s\bar{s}}^{(\lambda)}$$
$$\times \Psi^{\mathrm{full}}(\mathbf{P};\mathbf{x},\bar{\mathbf{x}})|q(\mathbf{x})_s^c\rangle|\bar{q}(\bar{\mathbf{x}})_{\bar{s}}^{\bar{c}}\rangle\,, \quad (A1)$$

where $\delta_{c\bar{c}}/\sqrt{3}$ and $\chi_{s\bar{s}}^{(\lambda)}$ are color and spin wave functions respectively. The spin wave function is normalized to unity:

$$\sum_{s\bar{s}} \chi_{s\bar{s}}^{(\lambda')*} \chi_{s\bar{s}}^{(\lambda)} = \delta_{\lambda\lambda'}\,. \quad (A2)$$

The complete coordinate-space wave function Ψ^{full} can be written as a plane wave in the c.m. momentum $\mathbf{P}$ times the relative quark-antiquark wave function,

$$\Psi^{\text{full}}(\mathbf{P};\mathbf{x},\bar{\mathbf{x}}) = \frac{e^{i\mathbf{P}\cdot\mathbf{X}_{\text{c.m.}}}}{(2\pi)^{3/2}}\,\Psi(\mathbf{x}_{\text{rel}})\ , \tag{A3}$$

where

$$\mathbf{x}_{\text{rel}} = \mathbf{x} - \bar{\mathbf{x}} \tag{A4}$$

and for the equal-mass case considered in this paper

$$\mathbf{X}_{\text{c.m.}} = (\mathbf{x} + \bar{\mathbf{x}})/2\ . \tag{A5}$$

We normalize the relative wave function $\Psi(\mathbf{x}_{\text{rel}})$ to unity:

$$\int d^3 x_{\text{rel}}\,|\Psi(\mathbf{x}_{\text{rel}})|^2 = 1\ . \tag{A6}$$

As the scattering amplitudes we calculate in this paper are functions of momenta, it is useful to transform this coordinate-space meson wave function into momentum space before evaluating scattering amplitudes. The full momentum-space wave function Φ^{full} is related to the coordinate-space wave function by

$$\Phi^{\text{full}}(\mathbf{P};\mathbf{k},\bar{\mathbf{k}}) = \frac{1}{(2\pi)^3}\iint d^3x\,d^3\bar{x}\,e^{-i\mathbf{k}\cdot\mathbf{x} - i\bar{\mathbf{k}}\cdot\bar{\mathbf{x}}}$$
$$\times\,\Psi^{\text{full}}(\mathbf{P};\mathbf{x},\bar{\mathbf{x}})\ . \tag{A7}$$

As the full coordinate-space wave function is a plane wave in the c.m. coordinate, the full momentum-space wave function is a c.m. momentum-conserving delta function times a relative-momentum wave function Φ:

$$\Phi^{\text{full}}(\mathbf{P};\mathbf{k},\bar{\mathbf{k}}) = \delta(\mathbf{P} - \mathbf{k} - \bar{\mathbf{k}})\,\Phi(\mathbf{k} - \bar{\mathbf{k}})\ . \tag{A8}$$

The relation between the relative wave functions $\Psi(\mathbf{x}_{\text{rel}})$ and $\Phi(\mathbf{k} - \bar{\mathbf{k}})$ follows from these results, and is

$$\Phi(\mathbf{k} - \bar{\mathbf{k}}) = \frac{1}{(2\pi)^{3/2}}\int d^3x_{\text{rel}}\,e^{-\frac{1}{2}(\mathbf{k}-\bar{\mathbf{k}})\cdot\mathbf{x}_{\text{rel}}}\,\Psi(\mathbf{x}_{\text{rel}}) \tag{A9}$$

with the inverse relation

$$\Psi(\mathbf{x}_{\text{rel}}) = \frac{1}{(2\pi)^{3/2}}\int d^3\left(\frac{\mathbf{k}-\bar{\mathbf{k}}}{2}\right)e^{+\frac{1}{2}(\mathbf{k}-\bar{\mathbf{k}})\cdot\mathbf{x}_{\text{rel}}}\,\Phi(\mathbf{k}-\bar{\mathbf{k}})\ . \tag{A10}$$

The normalization quoted above for Ψ also implies a normalization for Φ, which is

$$\int d^3p\,|\Phi(2\mathbf{p})|^2 = 1\ . \tag{A11}$$

The integral of $\Phi(2\mathbf{p})$ over $\mathbf{p}$ appears in several of the Born amplitudes; this is a special case of the Fourier relations above and gives the relative spatial wave function at contact:

$$\int d^3p\,\Phi(2\mathbf{p}) = (2\pi)^{3/2}\,\Psi(0)\ . \tag{A12}$$

In our evaluation of overlap integrals in the text we used Gaussian wave functions for illustration in several

examples. These are defined by

$$\Phi(\mathbf{k} - \bar{\mathbf{k}}) = \eta\,\exp\left\{-\frac{\lambda}{2}\,(\mathbf{k} - \bar{\mathbf{k}})^2\right\}\ , \tag{A13}$$

and our normalization convention gives

$$\eta = \sqrt{8}\,\left(\frac{\lambda}{\pi}\right)^{3/4}\ . \tag{A14}$$

The corresponding spatial wave function is

$$\Psi(\mathbf{x}_{\text{rel}}) = \left(\frac{\pi}{\lambda}\right)^{3/4}\exp\left\{-\frac{1}{8\lambda}\mathbf{x}_{\text{rel}}^2\right\}\ , \tag{A15}$$

so our Gaussian parameter λ is related to the usual simple-harmonic-oscillator (SHO) quark-model parameter β_{SHO} by

$$\lambda = \frac{1}{4\beta_{\text{SHO}}^2}\ . \tag{A16}$$

In light quark spectroscopy β_{SHO} is typically found to be about 0.3 GeV, although it is not strongly constrained by experiment; β_{SHO} values near 0.2 GeV have been used to describe form factors, and decays have required values near 0.4 GeV [30]. In our calculations we treat β_{SHO} and hence λ as a free parameter, with the understanding that realistic fitted values of β_{SHO} should not differ considerably from 0.3 GeV.

APPENDIX B: SPIN MATRIX ELEMENTS

The explicit examples of spin matrix elements we considered in the text were for $S_{\text{tot}} = 2$, $S_{\text{tot}}^z = 2$ meson-meson states, for which the $\mathbf{S}_i \cdot \mathbf{S}_j$ matrix elements were trivially $+1/4$ for all (i,j). In general the spin-spin matrix elements are nontrivial, since we are considering matrix elements between meson-meson states of definite S_{tot}, with (S_A, S_B) specified in the initial state, but with a crossed set (S_C, S_D) diagonal in the final state. This crossing also leads to nontrivial matrix elements for the spin identity operator I, which multiplies the Coulomb and linear Born amplitudes. In Table I we give these matrix elements for I and for the various spin-spin terms $\mathbf{S}_i \cdot \mathbf{S}_j$, which are labeled by the initial quark and antiquark indices. (For example, $\mathbf{S}_a \cdot \mathbf{S}_{\bar{b}}$ gives the "capture$_1$" matrix element.) The matrix elements are displayed with initial spins (S_A, S_B) horizontally and final spins (S_C, S_D) on the left margin of each table, and are separated according to $S_{\text{tot}} = 2$ (one channel), $S_{\text{tot}} = 1$ (three channels), and $S_{\text{tot}} = 0$ (two channels). We first give the "distinguishable quark" matrix elements, corresponding to the quark line diagram underlying the quark and gluon diagrams in (40)–(43), following which we give the matrix elements for the "symmetrizing" quark line diagram underlying (D4), which is also present if both the quarks and the antiquarks are identical.

TABLE I.   Matrix elements for I and various spin terms $S_i \cdot S_j$.

(1) Operator $= I$

	(1,1)
(1,1)	+1

	(1,1)	(1,0)	(0,1)
(1,1)	0	$-1/\sqrt{2}$	$+1/\sqrt{2}$
(1,0)	$-1/\sqrt{2}$	$+1/2$	$+1/2$
(0,1)	$+1/\sqrt{2}$	$+1/2$	$+1/2$

	(1,1)	(0,0)
(1,1)	$-1/2$	$-\sqrt{3}/2$
(0,0)	$-\sqrt{3}/2$	$+1/2$

(2) Operator $= S_a \cdot S_{\bar{b}}$, "capture$_1$"

	(1,1)
(1,1)	+1/4

	(1,1)	(1,0)	(0,1)
(1,1)	0	$-1/4\sqrt{2}$	$+1/4\sqrt{2}$
(1,0)	$-1/4\sqrt{2}$	$+1/8$	$+1/8$
(0,1)	$-3/4\sqrt{2}$	$-3/8$	$-3/8$

	(1,1)	(0,0)
(1,1)	$-1/8$	$-\sqrt{3}/8$
(0,0)	$+3\sqrt{3}/8$	$-3/8$

(3) Operator $= S_{\bar{a}} \cdot S_b$, "capture$_2$"

	(1,1)
(1,1)	+1/4

	(1,1)	(1,0)	(0,1)
(1,1)	0	$-1/4\sqrt{2}$	$+1/4\sqrt{2}$
(1,0)	$+3/4\sqrt{2}$	$-3/8$	$-3/8$
(0,1)	$+1/4\sqrt{2}$	$+1/8$	$+1/8$

	(1,1)	(0,0)
(1,1)	$-1/8$	$-\sqrt{3}/8$
(0,0)	$+3\sqrt{3}/8$	$-3/8$

(4) Operator $= S_a \cdot S_b$, "transfer$_1$"

	(1,1)
(1,1)	+1/4

	(1,1)	(1,0)	(0,1)
(1,1)	$-1/2$	$+1/4\sqrt{2}$	$-1/4\sqrt{2}$
(1,0)	$+1/4\sqrt{2}$	$-1/8$	$+3/8$
(0,1)	$-1/4\sqrt{2}$	$+3/8$	$-1/8$

	(1,1)	(0,0)
(1,1)	$+5/8$	$+\sqrt{3}/8$
(0,0)	$+\sqrt{3}/8$	$+3/8$

TABLE I. *(Continued).*

(5) Operator $= \mathbf{S}_{\bar{a}} \cdot \mathbf{S}_{\bar{b}}$, "transfer$_2$"

	(1,1)
(1,1)	+1/4

	(1,1)	*(1,0)*	*(0,1)*
(1,1)	+1/2	$+1/4\sqrt{2}$	$-1/4\sqrt{2}$
(1,0)	$+1/4\sqrt{2}$	+3/8	−1/8
(0,1)	$-1/4\sqrt{2}$	−1/8	+3/8

	(1,1)	*(0,0)*
(1,1)	+5/8	$+\sqrt{3}/8$
(0,0)	$+\sqrt{3}/8$	+3/8

(6) Operator $= I$, symmetrizing diagram

	(1,1)
(1,1)	+1

	(1,1)	*(1,0)*	*(0,1)*
(1,1)	0	$+1/\sqrt{2}$	$-1/\sqrt{2}$
(1,0)	$+1/\sqrt{2}$	+1/2	+1/2
(0,1)	$-1/\sqrt{2}$	+1/2	+1/2

	(1,1)	*(0,0)*
(1,1)	−1/2	$-\sqrt{3}/2$
(0,0)	$-\sqrt{3}/2$	+1/2

(7) Operator $= \mathbf{S}_a \cdot \mathbf{S}_{\bar{b}}$, "capture$_1$," symmetrizing diagram

	(1,1)
(1,1)	+1/4

	(1,1)	*(1,0)*	*(0,1)*
(1,1)	0	$+1/4\sqrt{2}$	$-1/4\sqrt{2}$
(1,0)	$-3/4\sqrt{2}$	−3/8	−3/8
(0,1)	$-1/4\sqrt{2}$	+1/8	+1/8

	(1,1)	*(0,0)*
(1,1)	−1/8	$-\sqrt{3}/8$
(0,0)	$+3\sqrt{3}/8$	−3/8

(8) Operator $= \mathbf{S}_{\bar{a}} \cdot \mathbf{S}_b$, "capture$_2$," symmetrizing diagram

	(1,1)
(1,1)	+1/4

	(1,1)	*(1,0)*	*(0,1)*
(1,1)	0	$+1/4\sqrt{2}$	$-1/4\sqrt{2}$
(1,0)	$+1/4\sqrt{2}$	+1/8	+1/8
(0,1)	$+3/4\sqrt{2}$	−3/8	−3/8

	(1,1)	*(0,0)*
(1,1)	−1/8	$-\sqrt{3}/8$
(0,0)	$+3\sqrt{3}/8$	−3/8

TABLE I. *(Continued)*.

(9) Operator $= \mathbf{S}_a \cdot \mathbf{S}_b$, "transfer$_1$," symmetrizing diagram

	(1,1)
(1,1)	+1/4

	(1,1)	*(1,0)*	*(0,1)*
(1,1)	+1/2	$-1/4\sqrt{2}$	$+1/4\sqrt{2}$
(1,0)	$-1/4\sqrt{2}$	+3/8	$-1/8$
(0,1)	$+1/4\sqrt{2}$	$-1/8$	+3/8

	(1,1)	*(0,0)*
(1,1)	+5/8	$+\sqrt{3}/8$
(0,0)	$+\sqrt{3}/8$	+3/8

(10) Operator $= \mathbf{S}_{\bar{a}} \cdot \mathbf{S}_{\bar{b}}$, "transfer$_2$," symmetrizing diagram

	(1,1)
(1,1)	+1/4

	(1,1)	*(1,0)*	*(0,1)*
(1,1)	$-1/2$	$-1/4\sqrt{2}$	$+1/4\sqrt{2}$
(1,0)	$-1/4\sqrt{2}$	$-1/8$	+3/8
(0,1)	$+1/4\sqrt{2}$	+3/8	$-1/8$

	(1,1)	*(0,0)*
(1,1)	+5/8	$+\sqrt{3}/8$
(0,0)	$+\sqrt{3}/8$	+3/8

APPENDIX C: DIRECT DIAGRAM EVALUATION

In this appendix we present simple diagrammatic rules for evaluating the spatial overlap integrals discussed in detail in the text. As a specific example we consider the "capture$_1$" diagram with a contact hyperfine interaction. Recall that this diagram

capture$_1$
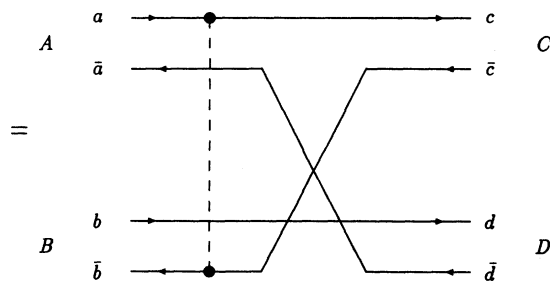
(C1)

was found in (65) to give the spatial overlap integral

$$I_{\text{space}} = -\frac{8\pi\alpha_s}{3m_q^2} \frac{\Psi_C^*(0)}{(2\pi)^{3/2}} \int d^3k \Phi_D^*(2k - A)$$

$$\times \Phi_A(2k + C)\Phi_B(2k - C) ,$$

(C2)

which is the matrix element of the spatial part of

$$H_I(\text{capture}_1) = -\frac{8\pi\alpha_s}{3m_q^2} \mathbf{S}_a \cdot \mathbf{S}_{\bar{b}} \, \delta(\mathbf{r}_{a\bar{b}}) .$$

(C3)

This interaction has already had the color degree of freedom $(\lambda/2)(-\lambda^T/2)$ removed as part of the "color factor." The "spatial part" is defined as the multiplier of the spin-spin factor $\mathbf{S}_a \cdot \mathbf{S}_{\bar{b}}$, which is $(-8\pi\alpha_s/3m_q^2) \, \delta(\mathbf{r}_{a\bar{b}})$.

To evaluate the spatial overlap integral for this diagram by inspection, we begin by writing a product of the four external-meson wave functions,

$$\Phi_A(a - \bar{a}) \ \Phi_B(b - \bar{b}) \ \Phi_C^*(c - \bar{c}) \ \Phi_D^*(d - \bar{d}) ,$$

(C4)

since the scattering amplitude will be proportional to this expression with appropriate relations imposed between the quark and antiquark momenta. We next substitute

for momenta which are redundant due to delta-function constraints; first we eliminate all the antiquark momenta, since each of these is equal to the corresponding external-meson momentum minus the quark momentum:

$$\bar{a} = A - a \ , \tag{C5}$$

$$\bar{b} = B - b \ , \tag{C6}$$

$$\bar{c} = C - c \ , \tag{C7}$$

$$\bar{d} = D - d \ . \tag{C8}$$

Substitution into the wave-function product gives

$$\Phi_A(2a - A) \ \Phi_B(2b - B) \ \Phi_C^*(2c - C) \ \Phi_D^*(2d - D) \ . \tag{C9}$$

Specializing to the "capture$_1$" diagram, there are additional momentum constraints due to the unscattered lines, which are

$$\bar{d} = \bar{a} \tag{C10}$$

and

$$d = b \ . \tag{C11}$$

Since we have already eliminated the antiquark momenta, these are equivalent to

$$d = a - A + D \tag{C12}$$

and

$$b = a - A + D \ , \tag{C13}$$

respectively. On substituting these identities in the wave-function product we obtain

$$\Phi_A(2a - A) \ \Phi_B(2a - 2A - B + 2D)$$

$$\times \Phi_C^*(2c - C) \ \Phi_D^*(2a - 2A + D) \ . \tag{C14}$$

As we evaluate these integrals in the c.m. frame, we may substitute $B = -A$ and $D = -C$ for the external-meson three-momenta, which gives

$$\Phi_A(2a - A) \ \Phi_B(2a - A - 2C)$$

$$\Phi_C^*(2c - C) \ \Phi_D^*(2a - 2A - C) \ . \tag{C15}$$

In the actual scattering amplitude there are initially eight momentum integrations over the four quark and four antiquark momenta, $a, b, c, d, \bar{a}, \bar{b}, \bar{c},$ and $\bar{d}$. Four of these momentum integrations (over $\bar{a}$, $\bar{b}$, $\bar{c}$, and $\bar{d}$) are trivial due to delta-function constraints in the external wave functions, and two more integrations (over b and d) also encounter delta-function constraints, due to unscattered lines in the matrix element. This leaves two unconstrained momenta to integrate over, which in this case are a and c. On replacing these implicit integrations we have

$$\iint d^3a \ d^3c \ \Phi_A(2a - A) \ \Phi_B(2a - A - 2C)$$

$$\Phi_C^*(2c - C) \ \Phi_D^*(2a - 2A - C) \ . \tag{C16}$$

This can be simplified by translating the variables of integration, $c \to c + C/2$ and $a \to a + (A + C)/2$, which gives

$$\left\{ \int d^3c \ \Phi_C^*(2c) \right\}$$

$$\times \left\{ \int d^3a \ \Phi_D^*(2a - A)\Phi_A(2a + C)\Phi_B(2a - C) \right\} \ . \tag{C17}$$

As a final simplification, note that the integral of $\Phi_C^*(2c)$ over c is proportional to the spatial wave function of meson C at contact (see Appendix A), so our result can be written as

$$\left\{ (2\pi)^{3/2} \Psi_C^*(0) \right\}$$

$$\times \left\{ \int d^3a \ \Phi_D^*(2a - A) \ \Phi_A(2a + C) \ \Phi_B(2a - C) \right\} \ . \tag{C18}$$

This is the wave-function integral for the diagram "capture$_1$" given at the beginning of this appendix. It remains to restore the overall constant $-8\pi\alpha_s/3m_q^2$ which multiplies the spin-spin Hamiltonian (C3) as well as the factor of $1/(2\pi)^3$ in (63), which arises from a plane-wave integral when the spin-spin Hamiltonian (or any of the other interactions) is transformed into momentum space [see equations (66-69)]. On restoring these multiplicative constants, we find

$$I_{\text{space}} = -\frac{8\pi\alpha_s}{3m_q^2} \cdot \frac{1}{(2\pi)^3}(2\pi)^{3/2}\Psi_C^*(0) \int d^3a \ \Phi_D^*(2a - A) \ \Phi_A(2a + C) \ \Phi_B(2a - C) \ , \tag{C19}$$

which is the result [(65), (C2)] derived in the text.

The factorization of the matrix element (C16) into the product of two integrals (C17) results from our assumption of a contact interaction. For noncontact interactions such as the Coulomb and linear terms or a "regularized" spin-spin interaction, the spatial matrix element involves the Fourier transform of the interaction in a generalized convolution integral, and no longer factorizes. In the case of the capture$_1$ diagram we have used for illustration, replacing the delta function in (C3) by a general function $v(r_{a\bar{b}})$ leads to the spatial overlap integral

$$I_{\text{space}} = -\frac{8\pi\alpha_s}{3m_q^2} \cdot$$

$$\iint d^3a\, d^3c\ \Phi_A(2a - A)\ \Phi_B(2a - A - 2C)$$

$$\times V(|\mathbf{a} - \mathbf{c}|)\ \Phi_C^*(2c - C)\ \Phi_D^*(2a - 2A - C)\ ,\quad (C20)$$

where $V(|\mathbf{p}|)$ is the Fourier transform of the spatial interaction $v(r_{a\bar{b}})$, normalized to

$$V(|\mathbf{p}|) = \frac{1}{(2\pi)^3} \int d^3x\ e^{i\mathbf{P}\cdot\mathbf{x}}\ v(r)\ . \quad (C21)$$

The generalization of the other capture diagram and the transfer diagrams to noncontact interactions is immediately obvious and can also be read directly from the scattering diagrams, with the factor of $1/(2\pi)^3$ being replaced by the Fourier transform of the potential between the scattering constituents. The momentum argument in V is simply the modulus of the momentum transfer between scattering constituents. One should be careful to avoid evaluating individual diagrams with long-range potentials, however; for linear potentials in particular one should only evaluate sums of diagrams which represent color-singlet scattering amplitudes, as the individual scattering diagrams will be infrared divergent. The h_{fi} amplitudes for these Coulomb and linear potentials are given explicitly in Section III D of the text.

APPENDIX D: APPLICATION TO IDENTICAL QUARKS

The Born formalism may be applied to systems having identical quarks and antiquarks, which leads to additional diagrams that arise from permutations of identical particle lines in scattering. One might *a priori* anticipate that antisymmetrization of asymptotic states is required when identical fermions are present in different hadrons. This is actually not required, since antisymmetrization (or symmetrization for bosons) is simply a bookkeeping device which prevents overcounting of equivalent states, and ensures for example that $|f_2 f_1\rangle$ is not counted as independent of $|f_1 f_2\rangle$. If the identical fermions are uniquely assigned an order in the state vector according to their quantum numbers, the "duplicate" state $|f_2 f_1\rangle$ is never admitted as a possibility, and the antisymmetrized state $(|f_1 f_2\rangle - |f_2 f_1\rangle)/\sqrt{2}$ need not be introduced. Since we order the quarks and antiquarks in the two-meson states according to the hadron they occupy asymptotically, we have uniquely specified the order in which fermions occur in the state vector, and need not antisymmetrize. This association of quarks with specific hadrons requires that we visualize the scattering in terms of asymptotically separate wave packets, but this presumably leads to scattering amplitudes which approach conventional plane-wave results as the wave packets become arbitrarily large.

Although identical fermions do not require explicit antisymmetrization of the asymptotic wave functions in meson-meson scattering, they do lead to additional scattering diagrams. To see this in the context of our $AB \to CD$ example, assume that both mesons have a u quark but that the antiquarks are different flavors (as in $\pi^+ K^+$ elastic scattering). The u quark initially in meson A can scatter into meson C *or* D, since both final mesons have a u quark. In our previous example with distinguishable quarks we *defined* meson C to be the final meson with the same quark as A, which gave a unique line diagram. With identical quarks however both $u_A \to u_C$ and $u_A \to u_D$ scattering processes are possible, so we have two line diagrams, one considered previously for distinguishable quarks and a new diagram which is obtained by exchanging the final quark lines. For the capture$_1$ process these diagrams are

$$\text{capture}_1 \quad = \tag{D1}$$

and

$$\text{capture}_1^{u-ex} \quad = \tag{D2}$$
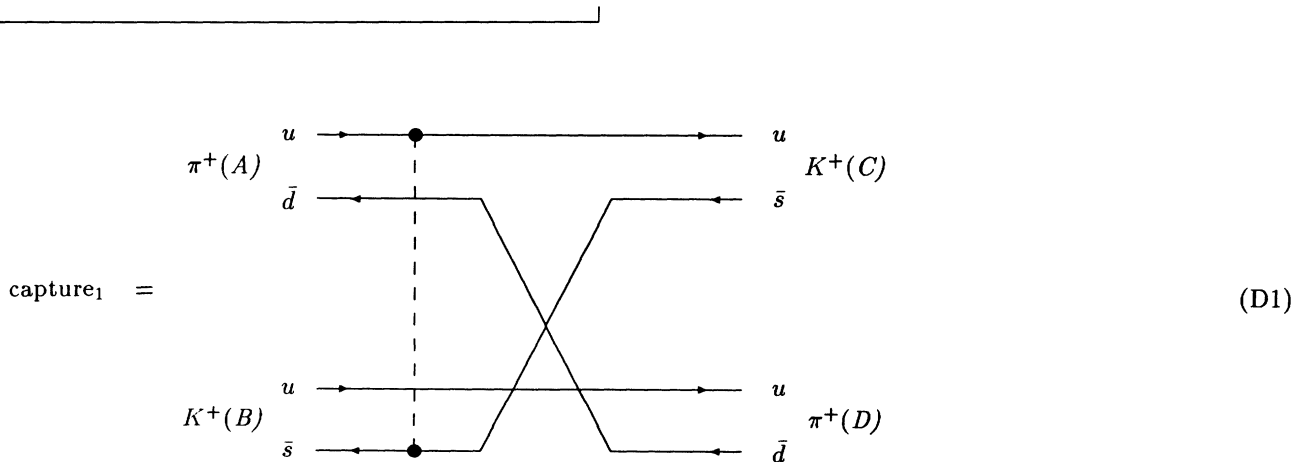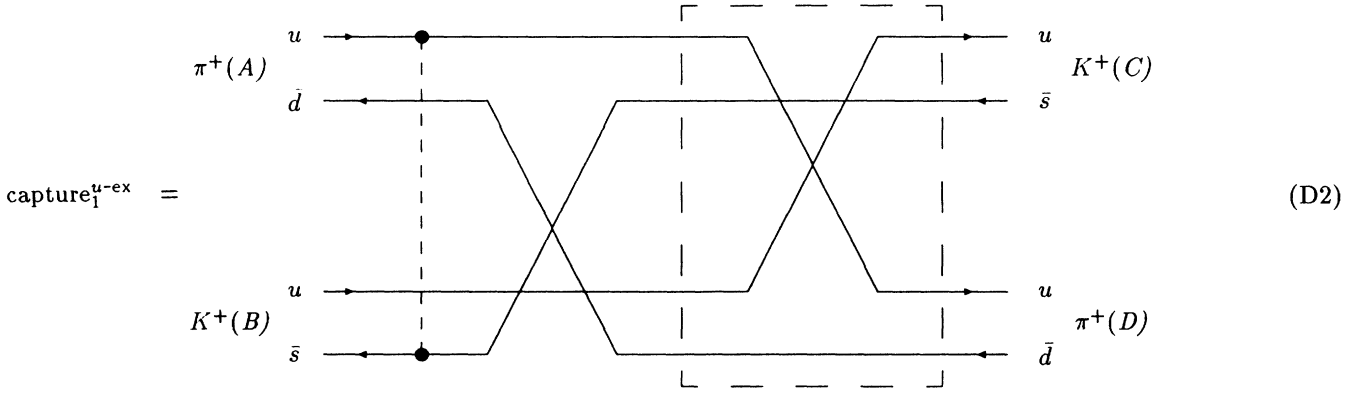
This new identical-quark line diagram evidently has a signature opposite to that of the first diagram, since it has a relatively odd number of line crossings. At the one-interaction level which we consider here, however, this new diagram actually vanishes due to a zero color factor. At first order in $\lambda \cdot \lambda$ one only encounters new nonvanishing identical-fermion contributions if both the quarks and antiquarks are identical, as in $\pi^+ \pi^+$ scattering. In this case one has the usual line diagram, a quark-exchange diagram as in (D2) which has a zero color factor, an antiquark-exchange diagram which also has a zero color factor (we do not show these two diagrams), and a nonzero quark-exchange plus antiquark-exchange diagram:

$$\text{capture}_1 \quad = \tag{D3}$$

and

$$\text{capture}_1^{symm} =$$

$$(D4)$$
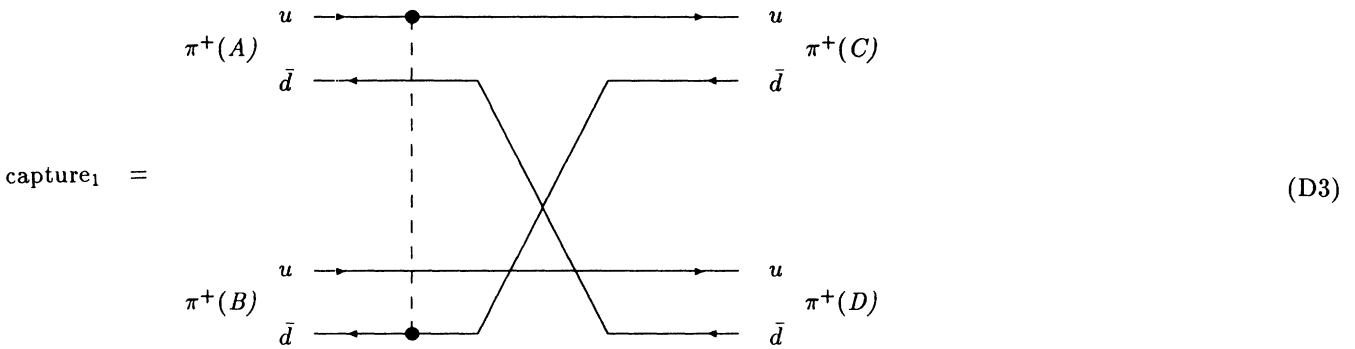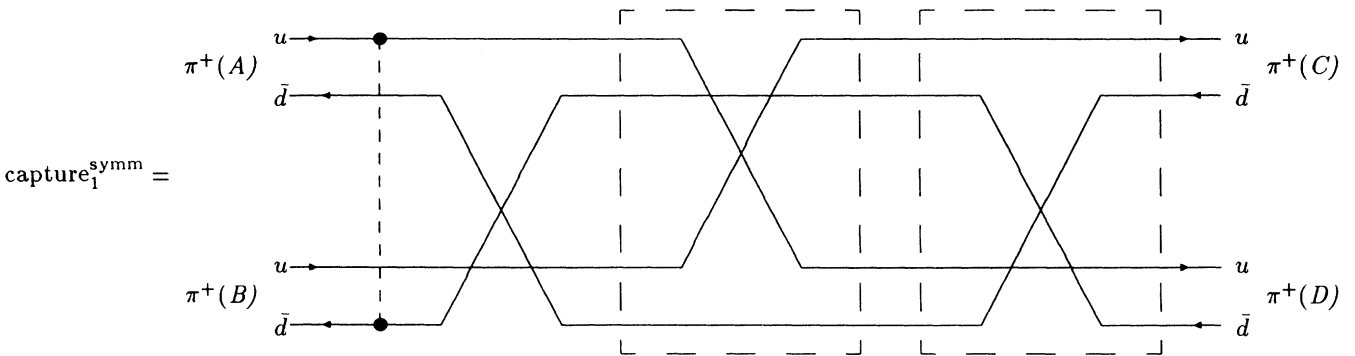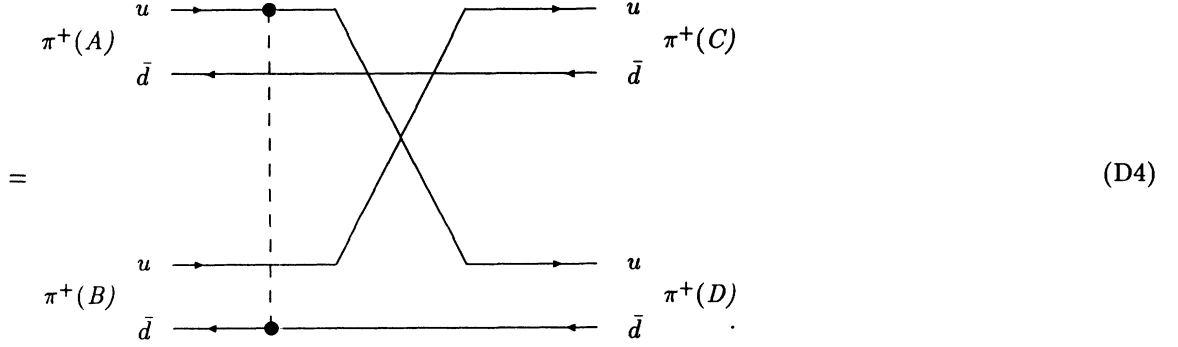
The new line diagram gives an amplitude with the same overall "signature" phase as the first diagram; this is expected because a quark pair *and* an antiquark pair have been exchanged relative to the first diagram. Detailed evaluation in the $S_{\text{tot}} = 2$ case (for a given $\lambda \cdot \lambda$ interaction between initial fermions) reveals that the new diagram is equal to the first diagram after exchange of C and D labels and momenta; for example, the "capture$_1$" diagram (D3) and corresponding identical quark- and antiquark-exchange diagram (D4) are

$$h_{fi}(\text{capture}_1) = -\frac{8\pi\alpha_s}{27m_q^2} \frac{\Psi_C^*(0)}{(2\pi)^{3/2}} \int d^3k \, \Phi_D^*(2\mathbf{k} - \mathbf{A}) \, \Phi_A(2\mathbf{k} + \mathbf{C}) \, \Phi_B(2\mathbf{k} - \mathbf{C}) \tag{D5}$$

and

$$h_{fi}^{\text{symm}}(\text{capture}_1) = -\frac{8\pi\alpha_S}{27m_q^2} \frac{\Psi_D^*(0)}{(2\pi)^{3/2}} \int d^3k \, \Phi_C^*(2\mathbf{k} - \mathbf{A}) \, \Phi_A(2\mathbf{k} - \mathbf{C}) \, \Phi_B(2\mathbf{k} + \mathbf{C}) , \tag{D6}$$

which evidently map into each other under exchange of C and D labels. (In the c.m. frame their momenta are related by $\mathbf{D} = -\mathbf{C}$.) We refer to the new identical fermion diagrams as in (D4) as "symmetrizing" diagrams because they impose Bose symmetry in the meson-meson scattering amplitude if the external mesons are identical.

APPENDIX E: MESON-MESON EQUIVALENT POTENTIALS

To study complicated hadron-hadron scattering problems with many open channels it is useful to approximate the meson-meson scattering amplitude by low-energy equivalent potentials. This allows a straightforward numerical study of the full system using the multichannel Schrödinger equation, which can easily incorporate physical meson masses and can be used to search for nonperturbative effects such as hadron-hadron bound states which are not directly accessible to our Born-order perturbative calculation. Here we shall give an explicit derivation of intermeson potentials which are equivalent to the Hamiltonian matrix element (74) near threshold.

Note first that this is an inexact procedure. The Hamiltonian matrix element h_{fi} is a function of both s and t, whereas a pure potential leads only to t dependence, so we can only approximate the matrix element h_{fi} (74) using a potential. We will describe two methods for deriving low-energy "equivalent potentials" which give scattering amplitudes approximately equal to h_{fi} near threshold. The first method has the advantage of simplicity, but produces a singular delta-function potential for our example; the second technique is more complicated, but can in principle be used to generate nonlocal potentials which reproduce the original scattering amplitude to arbitrary accuracy. A third method which leads to comparable numerical results in the $\pi\pi$ case has been discussed elsewhere by Swanson [25].

In our first technique we simply set s equal to its threshold value of $4M^2$, and determine the meson-meson potential that leads to the threshold matrix element

$$h_{fi}(s = 4M^2, t) = +\frac{8\pi\alpha_s}{27m_q^2} \frac{1}{(2\pi)^3} \left[\exp\left\{ \frac{\lambda t}{2} \right\} + \exp\left\{ -\frac{\lambda t}{2} \right\} - \frac{16}{3\sqrt{3}} \right] . \tag{E1}$$

Note also that these are in general "transition potentials" rather than diagonal ones, since the effect of the interaction is to transform the incoming (A, B) meson pair into a possibly different (C, D) final pair. The order of the final pair is actually important; to reproduce both rising and falling t dependences in (E1) it is convenient to introduce separate $(A \to C, B \to D)$ and $(A \to D, B \to C)$ potentials. In the $(A \to C)$ "t-channel potential" $V_t(r_{AB})$, the transferred momentum squared in $t = -(\mathbf{A} - \mathbf{C})^2$, whereas in the $(A \to D)$ "u-channel potential" it is $u = -(\mathbf{A} - \mathbf{D})^2$. The exponential $e^{\lambda t/2}$ is most easily identified with a t-channel potential,

$$
V_t(r) \quad = \qquad\qquad\qquad\qquad\qquad\qquad\qquad\qquad\qquad \text{(E2)}
$$

whereas the $e^{\lambda u/2} = e^{-\lambda t/2}$ terms, which would require a singular t-channel potential, can be directly identified with a u-channel potential,

$$
V_u(r) \quad = \qquad\qquad\qquad\qquad\qquad\qquad\qquad\qquad\qquad \text{(E3)}
$$

We divide the t-independent "capture diagram" contribution equally between these two potentials, which makes them the same function of r. The t-channel potential corresponding to (E1) is

$$
V_t(r) = \int d^3q \, e^{i\mathbf{q}\cdot\mathbf{x}} \, h_{fi}(s = 4M^2, t = -\mathbf{q}^2)
$$

$$
= \frac{8\pi\alpha_s}{27m_q^2} \left[\frac{e^{-r^2/2\lambda}}{(2\pi\lambda)^{3/2}} - \frac{8}{3\sqrt{3}}\delta(\mathbf{x}) \right] . \qquad \text{(E4)}
$$

We have written the transfer-diagram Gaussian with a coefficient that integrates to unity, so it can be compared directly to the capture-diagram delta function. One can see that their contributions are comparable and interfere destructively, so $S_{\mathrm{tot}} = 2$ vector-vector elastic scattering through the spin-spin hyperfine term is found to be relatively weak near threshold. In a numerical study using these potentials it would of course be necessary to replace the delta-function contribution by a finite-width distribution such as a narrow Gaussian.

If we are studying an identical-meson system, as in $\rho^+\rho^+$ elastic scattering, one need only introduce a single intermeson potential $V(r) = V_t(r) = V_u(r)$, because the u-channel contribution will automatically be introduced by the potential scattering formalism as a crossed meson diagram. There is in addition an overall factor of 2 in h_{fi} due to additional identical quark diagrams, as was explained in Appendix D. For $\rho^+\rho^+$ with $S_{\mathrm{tot}} = 2$ this gives

$$
V^{\rho^+\rho^+}(r) = \frac{16\pi\alpha_s}{27m_q^2} \left[\frac{e^{-r^2/2\lambda}}{(2\pi\lambda)^{3/2}} - \frac{8}{3\sqrt{3}}\delta(\mathbf{x}) \right] \qquad \text{(E5)}
$$

and the corresponding $I = 2 \; \pi\pi$ (and $I = 1 \; K\bar{K}$) potentials are

$$
V^{\pi^+\pi^+}(r) = \frac{8\pi\alpha_s}{9m_q^2} \left[\frac{e^{-r^2/2\lambda}}{(2\pi\lambda)^{3/2}} + \frac{8}{3\sqrt{3}}\delta(\mathbf{x}) \right] . \qquad \text{(E6)}
$$

This pseudoscalar-pseudoscalar interaction is relatively large because the capture and transfer diagrams contribute with the same sign. The positive effective potential corresponds to a repulsive interaction, consistent with the negative $I = 2 \; \pi\pi$ phase shift observed experimentally.

The second technique for generating equivalent potentials in $2 \to 2$ scattering was introduced by Barnes and Ghandour [23]. In this approach we begin with a scattering amplitude [such as $h_{fi}(s, t)$] which is a known function of s and t, and write it in terms of the exchanged three-momentum $\mathbf{q}$,

$$
\mathbf{q} = \mathbf{C} - \mathbf{A} , \qquad \text{(E7)}
$$

and a total t-channel momentum $\mathbf{P}$,

$$
\mathbf{P} = \frac{1}{2}(\mathbf{A} + \mathbf{C}) \qquad \text{(E8)}
$$

in the Breit frame. For our equal-mass scattering problem this simply substitutes

$$
t = -\mathbf{q}^2 \qquad \text{(E9)}
$$

and

$$s = 4M^2 + q^2 - 4P \cdot q + 4P^2 \qquad (E10)$$

for s and t. One then expands this scattering amplitude in a power series in P. The leading term is a function of q only, which when Fourier transformed gives the corresponding local potential

$$V(r) = \int d^3q\, e^{i q \cdot x}\, h_{fi}(s \to 4M^2 + q^2, t \to -q^2)\ . \qquad (E11)$$

The nonleading terms in the expansion of h_{fi}, which are proportional to $P_{i1} \cdots P_{in}$, give generalized potential operators with n external gradients ∇ multiplying functions of r. This technique, which might be termed a "locality expansion," generates the correct Breit-Fermi Hamiltonian at order $P_i P_j$ when applied to the one-photon-exchange Feynman amplitude [23].

When this technique is applied to the Gaussian h_{fi} (74) to generate a lowest-order local potential, the "transfer" diagrams give the same Gaussian potential found in (E6) using the first method, but the "capture diagram" delta function is replaced by a Gaussian with a different width. The resulting local t-channel potential is thus the sum of two Gaussians, and for the $I = 2\ \pi\pi$ and $I = 1$ KK systems is

$$V^{\pi^+\pi^+}(r) = \frac{64\alpha_s\beta_{\rm SHO}^3}{9\sqrt{\pi}m_q^2}\left[\frac{1}{2\sqrt{2}}e^{-2\beta_{\rm SHO}^2 r^2} + e^{-3\beta_{\rm SHO}^2 r^2}\right]\ . \qquad (E12)$$

(For our discussion we have written this as a function of $\beta_{\rm SHO}$ rather than $\lambda = 1/4\beta_{\rm SHO}^2$.) The KK potential has the same form and differs only in our choice of a larger quark mass for strange-nonstrange systems. This $I = 2\ \pi\pi$ potential is shown in Figure 5 for our standard light-quark parameter set $\alpha_s = 0.6$, $m_q = 0.33$ GeV, and $\beta_{\rm SHO} = 0.337$ GeV; with these parameters the repulsive core has a maximum value of
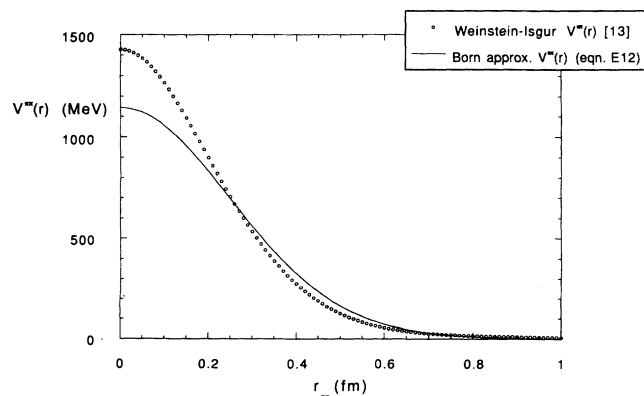
FIG. 5. Low-energy equivalent potentials for $I = 2\ \pi\pi$ scattering.

$$V^{\pi^+\pi^+}(0) = \frac{64\alpha_s\beta_{\rm SHO}^3}{9\sqrt{\pi}m_q^2}\left(\frac{1}{2\sqrt{2}} + 1\right) \approx 1.15\ {\rm GeV}\ , \qquad (E13)$$

and falls with a characteristic length scale of $r_0 \approx 0.5/\beta_{\rm SHO} \approx 0.3$ fm. The recent variational $I = 2\ \pi\pi$ potential of Weinstein and Isgur [14] is also displayed in Figure 5 for comparison, and is evidently very similar to our result. (Of course we do not expect exact agreement due to the systematic differences in our methods and parameters and our use of single-Gaussian external $q\bar{q}$ wave functions.) The Weinstein-Isgur $I = 2\ V^{\pi\pi}(r)$ potential we show in Figure 5 is their $I = 2\ \pi\pi$ potential as derived before they rescale it to give better agreement with experimental phase shifts. This is the $V_u^e(r)$ in Figure 3 of reference [13]. Note also that their corresponding KK and $s\bar{s}$-$s\bar{s}$ potentials $V_k^e(r)$ and $V_s^e(r)$ scale in overall magnitude approximately as m_q^{-2}, which is an exact result in our Born formalism assuming first-order scattering by the color-magnetic hyperfine term.

As we have used the Born approximation to define the equivalent potential $V(r)$ in terms of $h_{fi}(s,t)$, and also take the low-energy limit of h_{fi} to produce a local potential, we will only recover the original h_{fi} scattering amplitudes from $V(r)$ in the double limit of a weak potential near threshold. We have confirmed this for (E12) by comparing the analytic S-wave phase shift from h_{fi} (93) to the numerically evaluated phase shift due to (E12) in the double limit $\alpha_s \to 0$ and $s \to 4M^2$. For the physically relevant parameters of $\alpha_s = 0.6$ and $s > 4M^2$, however, there will be a discrepancy between the equivalent-potential phase shift predicted by (E12) and the original phase shift predicted by h_{fi}. As the multichannel Schrödinger equation studies of Weinstein and Isgur use similar equivalent potentials, it is especially interesting to test their internal consistency by comparing the original h_{fi} phase shift to the phase shift predicted by (E12) for $\pi\pi$ and KK parameters.

First we consider the less relativistic KK system. We showed the $I = 1$ KK phase shift predicted by h_{fi} in Figure 4. Using the same parameter set we numerically determined the phase shift predicted by the threshold-equivalent $I = 1$ KK potential (E12); this is shown together with the original h_{fi} phase shift in Figure 6. [This phase shift is determined by solving the nonrelativistic two-kaon Schrödinger equation with (E12), and is displayed as a function of $M_{KK} = 2\sqrt{M^2 + k^2}$.] Evidently the equivalent potential underestimates the S-wave KK phase shift somewhat, but is qualitatively correct and could be used in a multichannel Schrödinger formalism with little modification.

When we repeat this exercise for the $I = 2\ \pi\pi$ system (in Figure 7) we find a qualitatively different result; although the threshold-equivalent $V^{\pi\pi}(r)$ gives a phase shift similar to h_{fi} close to threshold, for $M_{\pi\pi} \gtrsim 0.4$ GeV it seriously underestimates the original h_{fi} phase shift. Apparently the pions are so relativistic that the s dependence of h_{fi} is quite important, and the low-energy potential formalism is inaccurate at experimentally relevant values of the $\pi\pi$ invariant mass. It appears likely
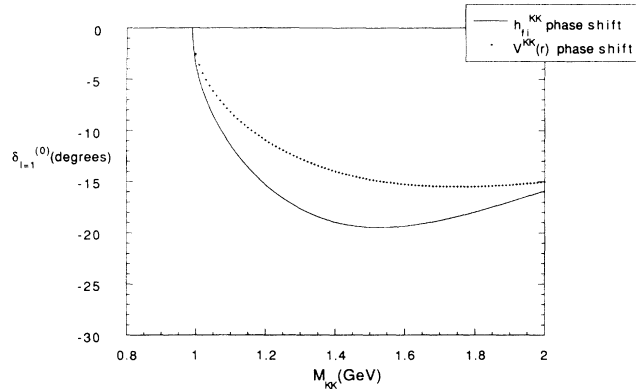
FIG. 6. Comparison of $K\bar{K}$ phase shifts due to $h_{f_i}^{K\bar{K}}$ and $V^{K\bar{K}}(r)$; $\alpha_s = 0.6$, $m_q = 0.44$ GeV, $\beta_{SHO} = 0.337$ GeV.

FIG. 7. Comparison of $h_{f_i}^{\pi\pi}$ and $V^{\pi\pi}(r)$ phase shifts.

that this is the origin of the underestimated S-wave $\pi\pi$ phase shift of Weinstein and Isgur, which is quite similar to the inaccurate phase shift our $V^{\pi\pi}(r)$ produces. (This is expected since our potentials are quite similar, as shown in Figure 5.) This suggests that their "rescaling" of $V^{\pi\pi}(r)$ was actually compensating for the inadequacy

of low-energy $\pi\pi$ potentials in describing relativistic $\pi\pi$ scattering amplitudes, and this rescaling should not be applied to less relativistic meson-meson systems such as $K\bar{K}$. An experimental determination of the $I = 1$ $K\bar{K}$ phase shift would be very useful as a test of this possibility.

[1] See, E. Fermi *Nuclear Physics* (University of Chicago Press, Chicago, 1950), for an early discussion, and S. DeBenedetti, *Nuclear Interactions* (Wiley, New York, 1964), Secs. 7.17 and 7.26c.

[2] S. Weinberg, Phys. Rev. Lett. **17**, 616 (1966).

[3] K.L. Au, D. Morgan, and M.R. Pennington, Phys. Rev. D **35**, 1633 (1987); D. Morgan and M.R. Pennington, Phys. Lett. B **258**, 444 (1991).

[4] See, for example, M. Lacombe, B. Loiseau, J.M. Richard, and R. Vinh Mau, Phys. Rev. C **21**, 861 (1980).

[5] See, for example, *Physics at LEAR with Low-Energy Cooled Antiprotons*, Proceedings of the International School of Physics of Exotic Atoms, Erice, Italy, 1982, edited by U. Gastaldi and R. Klapisch, Ettore Majorana International Science Series: Physical Sciences, Vol. 17 (Plenum, New York, 1984).

[6] N. Isgur, Acta Physica Austriaca Suppl. **XXVII**, 177 (1985).

[7] K. Shimizu, Rep. Prog. Phys. **52**, 1 (1989).

[8] D.A. Liberman, Phys. Rev. D **16**, 1542 (1977).

[9] C.E. DeTar, Phys. Rev. D **17**, 302 (1977); **17**, 323 (1977).

[10] K. Maltman and N. Isgur, Phys. Rev. Lett. **50**, 1827 (1983).

[11] R.L. Jaffe and F.E. Low, Phys. Rev. D **19**, 2105 (1979).

[12] See, for example, G.P. Lepage and S.J. Brodsky, Phys. Rev. D **22**, 2157 (1980), and the review by S.J. Brodsky and G.P. Lepage, in *Perturbative Quantum Chromodynamics*, edited by A. Muller (World Scientific, Singapore, 1989).

[13] J. Weinstein and N. Isgur, Phys. Rev. Lett. **48**, 659 (1982); Phys. Rev. D **27**, 588 (1983).

[14] J. Weinstein and N. Isgur, Phys. Rev. D **41**, 2236 (1990).

[15] S. Gardner and E.J. Moniz, Phys. Rev. C **36**, 2504 (1987); S. Gardner, *ibid.* **42**, 2193 (1990).

[16] See, for example, R.J. Eden, *High Energy Collisions of Elementary Particles* (Cambridge University Press, Cambridge, England, 1967); B.T. Feld, *Models of Elementary Particles* (Blaisdell, Waltham, 1969); S. Humble, *Introduction to Particle Production in Hadron Physics* (Academic, New York, 1974); S. Gasiorowicz, *Elementary Particle Physics* (Wiley, New York, 1966), p.481.

[17] P.V. Landshoff, Report No. CERN-TH.6277/91 (unpublished); and (personal communication); UA4 Collaboration, D. Bernard *et al.*, Phys. Lett. B **198**, 583 (1987); N. Amos *et al.*, Nucl. Phys. **B262**, 689 (1985).

[18] K. Dooley, E.S. Swanson, and T. Barnes, Phys. Lett. B **275**, 478 (1992); K. Dooley, in Hadron '91, Proceedings of the 4th International Conference on Hadron Spectroscopy, College Park, Maryland, 1991 (unpublished).

[19] N.A. Törnqvist, Phys. Rev. Lett. **67**, 556 (1991); in Hadron '91 [18].

[20] J.D. Bjorken and S.D. Drell, *Relativistic Quantum Fields* (McGraw-Hill, New York, 1965), Vol. 2, pp. 57–62.

[21] L.I. Schiff, *Quantum Mechanics* (McGraw-Hill, New York, 1968), pp. 384–387.

[22] Particle Data Group, J. J. Hernández *et al.*, Phys. Lett. B **239**, 1 (1990).

[23] T. Barnes and G.I. Ghandour, Phys. Lett. **118B**, 411 (1982).

[24] J.J. de Swart, Rev. Mod. Phys. **35**, 916 (1963); See also M. Gell-Mann and Y. Ne'eman, *The Eightfold Way* (Benjamin, Reading, MA, 1964); J.J.J. Kokkedee, *The Quark Model* (Benjamin, Reading, MA, 1969); F.E. Close, *An Introduction to Quarks and Partons* (Academic, New York, 1979); A. LeYaouanc, L. Oliver, O. Pène, and J.-C. Raynard, *Hadron Transitions in the Quark Model* (Gordon and Breach, New York, 1988).

[25] E.S. Swanson, Ann. Phys. (NY) (to be published).

[26] M.R. Pennington (personal communication).

[27] W. Hoogland *et al.*, Nucl. Phys. **B126**, 109 (1977).

[28] W.Ochs, Max-Plank-Institut Report No. MPI-Ph/Ph 91-35, 1991 (unpublished).

[29] J. Weinstein, University of Mississippi report, 1991 (unpublished).

[30] N. Isgur (personal communication).

[31] C.B. Dover and G.E. Walker, Phys. Rep. **89**, 1 (1982).